

Chitosan nano-vehicles as biocompatible delivering tools for a new Ag(I)curcuminoid-Gboxin analog complex in cancer and inflammation therapy

Serag Eldin I. Elbehairi, Lamia A. Ismail, Mohammad Y. Alfaifi, Reda F.M. Elshaarawy, Hani S. Hafez



PII: S0141-8130(20)34799-1

DOI: <https://doi.org/10.1016/j.ijbiomac.2020.10.153>

Reference: BIOMAC 17043

To appear in: *International Journal of Biological Macromolecules*

Received date: 12 August 2020

Revised date: 6 October 2020

Accepted date: 20 October 2020

Please cite this article as: S.E.I. Elbehairi, L.A. Ismail, M.Y. Alfaifi, et al., Chitosan nano-vehicles as biocompatible delivering tools for a new Ag(I)curcuminoid-Gboxin analog complex in cancer and inflammation therapy, *International Journal of Biological Macromolecules* (2018), <https://doi.org/10.1016/j.ijbiomac.2020.10.153>

This is a PDF file of an article that has undergone enhancements after acceptance, such as the addition of a cover page and metadata, and formatting for readability, but it is not yet the definitive version of record. This version will undergo additional copyediting, typesetting and review before it is published in its final form, but we are providing this version to give early visibility of the article. Please note that, during the production process, errors may be discovered which could affect the content, and all legal disclaimers that apply to the journal pertain.

**Title page****Chitosan Nano-vehicles as biocompatible delivering tools for a new Ag(I)curcuminoid-Gboxin analog complex in cancer and inflammation therapy**

Serag Eldin I. Elbehairi<sup>a,b</sup>, Lamia A. Ismail<sup>c</sup>, Mohammad Y. Alfaifi<sup>a</sup>, Reda F.M. Elshaarawy<sup>d,e,\*</sup>, Hani S. Hafez<sup>f,\*</sup>.

<sup>a</sup> Biology Department, Faculty of Science, King Khalid University, 9004 Abha, Saudi Arabia

<sup>b</sup> Cell Culture Lab, Egyptian Organization for Biological Products and Vaccines (VACSERA Holding Company), Giza 12311, Egypt<sup>c</sup> Faculty of Science, Zoology Department, Suez University, 43533 Suez, Egypt.

<sup>c</sup> Department of Chemistry, Faculty of Science, Port Said University, Port Said, Egypt.

<sup>d</sup> Institut für Anorganische Chemie und Strukturchemie, Heinrich-Heine Universität Düsseldorf, 40204 Düsseldorf, Germany.

<sup>e</sup> Faculty of Science, Chemistry Department, Suez University, 43533 Suez, Egypt.

<sup>f</sup> Faculty of Science, Zoology Department, Suez University, 43533 Suez, Egypt.

**Corresponding author:**

Email: [reda.elshaarawy@suezuniv.edu.eg](mailto:reda.elshaarawy@suezuniv.edu.eg).

[reel-001@hhu.de](mailto:reel-001@hhu.de)

Orcid ID: [0000-0003-2100-8928](https://orcid.org/0000-0003-2100-8928)

Email: [hani.hafez@suezuniv.edu.eg](mailto:hani.hafez@suezuniv.edu.eg)

**Abstract**

A novel anticancer and anti-inflammatory agent based on hybrid curcuminoid-Gboxin analog (FLLL49-GbA) and its nano-molecular silver(I) complex (Ag(I)FLLL49-GbA) have successfully synthesized. In addition, chitosan nanoparticles (CNPs) were used to encapsulate this macromolecular complex, targeting enhancing its therapeutic effect and minimizing its side impacts. The encapsulated Ag(I) complex was significantly triggered apoptosis ( $P < 0.05$ ) with much more rapidly release of Ag(I)FLLL49-GbA from the CNPs at pH 5.3 than at pH 7.4, which is beneficial for cancer-targeted drug delivery. Free complex showed promising ability in preventing glucose uptake and lactate production coupled with cellular ATP depletion in cancer cells. Additionally, there was significant decrease in the inflammatory cytokines in breast cancer (MCF-7) and lung cancer (A549) cells with values of  $P < 0.01$  and  $P < 0.001$  after 24 h incubation. Furthermore, the death-inducing proteins have been significantly up-regulated ( $P < 0.01$  to  $P < 0.001$ ) after 36 h incubation of cancer cells. Consequently, the novel curcuminoid macromolecule showed significant feasibility in triggering the high expression of apoptotic caspases caspase 3, caspase 8, P53, and Bax ( $P < 0.01$  to  $P < 0.001$ ) after 48 h of chemotherapy. Noteworthy, the cytotoxicity of Ag(I)FLLL49-GbA was significantly increased

toward cancer cells (MCF-7 > A549), while, reduced toward normal cells (HeLa) after loading on chitosan Nano-vehicles.

**Keywords:** Ag(I)-curcuminoid macromolecule-loaded Chitosan Nano-vehicles; Anticancer and Anti-inflammatory; Structure-function relationship.

## 1. Introduction

Cancer cells adjust their metabolism to generate all molecules and energy sources required to help the tumor to regulate its survival environment. Such metabolic features of cancer cells are believed to be a result of mutations in oncogenes and tumor suppressors that manage the cellular metabolism [1]. Natural therapeutics have been used for long periods for their persuasive role to inhibit cancer cell survival and progression. Amongst natural chemotherapeutics, curcumin (Cur) (1,7-Bis(4-hydroxy-3-methoxyphenyl)-hepta-1,6-dien-3,5-dione) has been demonstrated as one of the most anticancer agents with different therapeutic benefits against multiple chronic diseases [2]. Great efforts have been exerted to enhance the anticancer activity of Cur through the chemical refinement of its structure [3,4], to create many Cur derivatives, analogs, and conjugates [5,6]. Noteworthy that sustaining  $\alpha,\beta$ -unsaturated carbonyl segment in the Cur derivatives is an important issue, as it plays a pivotal role in the anticancer action of such compounds [7,8]. Among these derivatives, 1,7-Bis(3,4-dimethoxyphenyl)-4-cyclohexyl-hepta-1,6-dien-3,5-dione (FLLL32) and 1,7-Bis(4-hydroxy-3-methoxyphenyl)-4-cyclohexyl-hepta-1,6-dien-3,5-dione (FLLL49) (**Fig. 1**) were categorized as promising highly active anticancer agents [9,10]. These compounds have a great capacity to inhibit the Signal Transducer and Activator of Transcription 3 (STAT3) protein phosphorylation [9,10,11] which plays a significant role in the progression, proliferation, migration, invasion, metastasis, and survival of tumor cells [12,13,14]. Additionally, FLLL32 can reduce STAT3-DNA binding affinity and expression leading to, Osteosarcoma cell lines apoptosis [9]. However, unfortunately, the poor aqueous-solubility and rapid clearance of the bioactive Cur and Cur-based compounds prevent from reaching their maximum potential. Many strategies have been employed to tackle these challenges, particularly, coordination to metal ions which can be also used to mitigate the inherent drawbacks of Cur, such as promoted tolerance under physiological conditions. Moreover, metal complexes of Cur and its derivatives expand their potential applications, as compared to parent ligand, in cancer therapy [15]. Most notably, silver-based Cur and its derivatives that were emphasized to have multidiscipline biological applications such as; anticancer and anticancer drug delivery (Ex. ST06-AgNPs and Cur-AgNPs) [16,17,18], antiviral (Ex. Cur-AgNPs) [19], anti-biofilm (Ex. CurNPs-AgNPs) [20], wound dressing and antibacterial (Ex. Cur-AgNPs and Ag(I)Cur complex) [21,22].

Nanoparticles-based drug delivery systems (DDS) have gained extensive attention for their ability to improve the therapeutic index of drugs (bioavailability, chemical stability, selectivity) and reduce their adverse side effects [23]. Among DDS, polymeric nanoparticles (PNPs), particularly chitosan nanoparticles (CNPs), have categorized as promising drug carriers due to the non-toxicity, biocompatibility, biodegradability, and sustainable drug release [24,25]. To the name few, CPNs were

assigned as effective nanocarriers for versatile drugs including anticancer [25,26], antibiotics [25,27], anti-HIV medications [28], and.....etc. In addition, the CNPs have also been successfully used for the encapsulation of curcumin targeting diverse therapeutic applications [29,30].

Therefore, inhibition of glycolysis severely impairs the ATP generation and consequently prevents cancer cells to be highly dependent on this metabolic pathway for survival. Thus, great efforts in cancer therapy have targeted the glycolysis process as a therapeutic strategy to prevent the proliferation and survival of cancer cells, whereas inhibition of mitochondrial oxidative phosphorylation (OXPHOS) has remained largely unexplored. It noteworthy that a novel small molecule, 2-ethyl-1-(2-(((1*R*,3*R*,5*R*)-3-isopropyl-5-methylcyclohexyl)oxy)-2-oxoethyl)-3-methyl-1*H*-benzo[d]imidazol-3-ium chloride (Gboxin, Gb) (**Fig. S1**) was explored recently and assessed as a mitochondrial OXPHOS inhibitor [31].

Motivated by these aforesaid prominent facts and follow-up to our constant pursuit in exploring novel chemotherapeutic candidates [32,33,34]; the main objective of the current work is to fabricate novel anti-inflammatory and anticancer agents based on Gboxin analog (GbA) and curcuminoid derivative (FLLL49), (FLLL49-GbA conjugate) and its Ag<sub>2</sub>S complex. In addition, the capacities of these compounds to induce apoptosis in breast and lung cancer cells will be addressed. Moreover, exploiting the beneficial effects of CNPs as a sustainable delivering system for encapsulating Ag(I)LL49-GbA for cancer therapeutics.

## 2. Material and methods

Chemicals and starting materials used for the synthesis of our targeted materials (FLLL49, GbA, and CNPs) and different instrumental techniques utilized for full characterization of the fabricated materials were given in the electronic supplementary information (**ESI†**).

### 2.1. Chemistry

#### 2.1.1. Synthesis of the FLLL49-GbA conjugate

A solution of FLLL49 (0.87 g, 2.0 mmol) and GbA (1.96 g, 5.0 mmol) in anhydrous DCM (100 mL) was treated with 1-ethyl-3-(3-dimethylaminopropyl) carbodiimide (EDC) (1.15 g, 6 mmol) and 4-dimethylaminopyridine (DMAP) (0.73 g, 6 mmol) under stirring at room temperature (RT) and N<sub>2</sub> atmosphere. After stirring overnight at RT, a saturated aqueous NaHCO<sub>3</sub> solution (50 mL) was added to the reaction mixture. Then, the DCM layer was separated, and the aqueous phase was extracted with additional amounts of DCM (3 × 25 mL). The organic phases were collected and dried with anhydrous sodium sulfate. After evaporation to dryness under vacuum, the residue was subjected to column chromatography on silica gel (200–400 mesh) with a mixture of ethyl acetate/ n-hexane (1:2 V/V) as an eluent. The collected product was further recrystallized in a methanol-acetonitrile mixed solvent to afford pure compound FLLL49-GbA. Yield 78%, mp 124–125°C. FTIR (KBr, cm<sup>-1</sup>): 3027

(m, sh), 2995 (m, sh), 2877 (m, sh), 1734 (s, sh), 1674 (s, sh), 1580, 1534, 1466 (s, sh), 1379 (m, sh), 1150 (s, sh), 967 (m, sh), 736 (m, sh).  $^1\text{H}$  NMR (200 MHz, DMSO- $d_6$ ) 8.52 (d,  $J = 7.3$ , 2H), 8.37 (t,  $J = 7.2$ , 2H), 7.79 (dt,  $J = 4.6, 1.9$  Hz, 2H), 7.62 – 7.51 (m, 4H), 7.11 (dd,  $J = 15.5, 1.9$  Hz, 2H), 6.97 – 6.76 (m, 4H), 6.73 – 6.58 (m, 2H), 5.27 (s, 4H), 3.93 (s, 6H), 3.74 (s, 6H), 3.71 – 3.62 (m, 1H), 2.54 (q,  $J = 7.3$  Hz, 4H), 1.99 – 1.76 (m, 6H), 1.86 (s, 1H), 1.42 (t,  $J = 7.3$  Hz, 6H), 1.25 – 1.01 (m, 4H).  $^{13}\text{C}$  NMR (125 MHz, DMSO- $d_6$ )  $\delta$  (ppm): 201.34, 168.21, 157.14, 161.88, 143.41, 141.67, 132.16, 131.78, 131.24, 127.02, 126.72, 126.54, 124.83, 122.30, 113.74, 113.49, 111.63, 56.62, 51.91, 40.02, 39.83, 25.97, 23.61, 19.09, 15.34, 14.17. ESI-MS: in positive mode peaks at  $m/z$  874.45 ( $[\text{C}_{50}\text{H}_{54}\text{ClN}_4\text{O}_8]^+$ ,  $M - \text{Cl}^-$ ) a.m.u. and 419.1 ( $[\text{C}_{50}\text{H}_{54}\text{ClN}_4\text{O}_8]^{2+}$ ,  $M - 2 \text{Cl}^-$ ) a.m.u. Anal. Calcd. for  $\text{C}_{50}\text{H}_{54}\text{Cl}_2\text{N}_4\text{O}_8$  ( $M = 909.90$  g/mol): C, 66.00; H, 5.98; N, 6.16 %. Found: C, 65.94; H, 6.02; N, 5.98 %.

### 2.1.2. Synthesis of Ag(I)FLLL49-GbA complex

A solution of silver nitrate (0.50 g, 3.0 mmol) in acetonitrile (3 mL) was added dropwise with stirring to a solution of FLLL49-GbA (0.91 g, 1 mmol) in DMF (30 mL) at room temperature. After stirring this mixture overnight at RT, the resulting black solid was collected by filtration through a celite pad, washed several times with MeOH followed by diethyl ether, and dried in *vacuo* at RT. Yield 56%. FTIR (KBr,  $\text{cm}^{-1}$ ): 3432 (s, br), 3054 (m, sh), 2997 (m, sh), 2883 (m, sh), 1768 (s, sh), 1660 (s, sh), 1585, 1539, 1466 (s, sh), 1386 (m, sh), 1153 (s, sh), 956 (m, sh), 742 (m, sh), 526 (w, sh). Anal. Calcd. for  $\text{C}_{50}\text{H}_{54}\text{AgCl}_2\text{N}_5\text{O}_{11}$  ( $M = 1079.77$  g/mol): C, 55.62; H, 5.04; N, 6.49 %. Found: C, 54.98; H, 5.12; N, 6.38 %.

### 2.1.3. Synthesis of (Ag(I)FLLL49-GbA)CNPs

Initially, a clear chitosan (CS) solution (0.2% w/v) was prepared by dissolving CS in acetic acid (1% v/v), thereafter, a certain amount of Ag(I)FLLL49-GbA complex was added portion wise into 20 mL CS solution; the final concentration of Ag(I)FLLL49-GbA in CS solution is 0.5 mg/mL. After complete dispersion, the pH of mixture was adjusted to 6.0 by 0.25 M NaOH. After stirring for 30 min, a solution of a cross-linker sodium tripolyphosphate (TPP) (0.1% w/v) was added dropwise to this mixture under constant stirring (1000 rpm) at room temperature to achieve final mass ratios of 2.5:1 (CS:TPP). The suspension obtained was further stirred (1000 rpm) at the same temperature for 60 min and then centrifuged at 16000 rpm under ambient conditions for 30 min to isolate the nanoparticles ((Ag(I)FLLL49-GbA)CNPs) and supernatant. The isolated nanoparticles were washed thrice by deionized water and then dried by a further freeze-drying process in presence of 3% mannitol as a lyophilized protecting agent. The blank CNPs were prepared by a similar protocol but without the addition of Ag(I)FLLL49-GbA complex.

### 2.1.4. Determination of Ag(I)FLLL49-GbA loading and encapsulation efficiency of CNPs

The Ag(I)FLLL49-GbA complex loading and encapsulation efficacy may be calculated using two

previously reported methods [26,35], with slight modification. In the first indirect method, the unloaded Ag(I)FLLL49-GbA was measured, in the supernatant collected after centrifugation, using UV-vis spectrophotometer at 432 nm. On the other hand, the second experiment based on direct estimation of the Ag(I)FLLL49-GbA in the Nano-formulation ((Ag(I)FLLL49-GbA)CNP) through re-dispersion of this nanocomposite in milli-Q water (5 mL) and 40 mL of 0.1 M HCl solution under ultrasonic irradiation for 5 min. Thereafter, this mixture solution was layered with 40 mL of acetic ether twice. After layering, the content was evaporated under reduced pressure and the obtained residue was re-dissolved in DMSO (25 mL) for determination of Ag(I)FLLL49-GbA content using UV-vis spectrophotometer at 432 nm (with DMSO as blank control). The encapsulation and loading efficacies are calculated using equations (1, 2);

$$\text{Encapsulation efficacy (\%)} = \frac{W_{TC} - W_{UC}}{W_{TC}} \times 100 \quad (1)$$

$$\text{Loading efficacy (\%)} = \frac{W_{TC} - W_{UC}}{W_{CNPs}} \times 100 \quad (2)$$

where  $W_{TC}$  is the total weight of Ag(I)FLLL49-GbA complex added to the system;  $W_{UC}$  weight of un-encapsulated complex;  $W_{CNPs}$  is the weight of chitosan nanoparticles.

### 2.1.5. *In vitro* release of Ag(I)FLLL49-GbA from chitosan nanoparticles (CNPs).

The Ag(I)FLLL49-GbA-loaded chitosan Nano-formulation ((Ag(I)FLLL49-GbA)CNP) (0.5 mg) was dispersed in phosphate-buffered saline (PBS) (pH 7.4) or acetate buffer (ABS) (pH 5.3) (3 mL) and subsequently dialyzed into a dialysis bag (cut-off 5 kDa) against 40 mL of a mixture of 30% ethanol and 70% ABS pH 5.3 or PBS 7.4 as a release medium. The content was stored in a 37 °C and 150 rpm shaker incubator. At fixed time intervals, 1 mL samples were drawn and replaced with fresh medium by equal volume. Each sample was supplemented with 4 mL ethanol and analyzed at 432 nm against null medium UV spectrophotometers for measuring Ag(I)FLL49-GbA release concentration. The complex discharge fraction was determined based on the initial amount of Ag(I)FLL49-GbA with nanoparticles. The following equation was used to estimate the cumulative release of Ag(I) complex from CNPs. The cumulative release of Ag(I) complex was calculated using equation (3);

$$\text{Cumulative release (\%)} = \frac{E}{E^o} \times 100 \quad (3)$$

Where  $E^o$  and  $E$  are the initially loaded and release amount of Ag(I)FLL49-GbA from the encapsulated form in medium, respectively.

## 2.2. Anticancer study

### 2.2.1. Cell culture

The human breast (MCF-7) and lung (A549) cancer cells were provided by VACSERA Tissue Culture Unit. The cell lines were cultivated in Dulbecco's Modified Eagle Medium (DMEM, Gibco) and supplemented with a fetal bovine serum (FBS, 10%) (TBD Science), all the contents have been

incubated overnight at 37°C under 5% CO<sub>2</sub> atmosphere.

Additionally, the biological assessments of the curcumioid derivatives activity against tumor cells have been carried out using their free form. While, encapsulated complex nano-chitosan form ((Ag(I)FLLL49-GbA)CNPs) activity has been tested against their action for inducing different apoptosis stages using the DNA binding dyes Acridine orange (AO) and Ethidium bromide (EtBr).

### **MTT assay**

MTT assay has been carried out to testify the cell viability of the treated breast carcinoma (MCF-7) and lung carcinoma (A549) cells using colorimetric activities of the yellow MTT (3-(4,5-dimethylthiazol-2-yl)-2,5-diphenyltetrazolium bromide), each experiment was carried out using 5 replicates.  $2 \times 10^3$  cells were implanted into a 96-well DMEM-containing platform, and 10% FBS was implanted in a humidified atmosphere of 5% CO<sub>2</sub> at 37 °C for 24 h. The culture medium was replaced with 200 µL treating medium containing serial concentrations of tested substances and incubated overnight, followed by addition of 20 µL (5 mg/mL, Sigma) of MTT solution. Afterward, the medium has been carefully discarded and followed by the addition of 200 µL DMSO and agitated for 10 mins to be ready for colorimetric reading at 490 nm using a microplate reader (Multiskan-Thermo Scientific).

### **2.3. Glucose uptake measurement**

The estimation of glucose uptake by cancer cells (MCF-7 and A549) has been detected through the enzymatic NADPH-amplifying machine for 2-deoxyglucose. Briefly, cells have been seeded into 5-well plates and incubated overnight in Gibco™ RPMI 1640 Medium (cat no# 11875101) supplemented with 11mM glucose, 1% penicillin/streptomycin (Mediatech), and 10% fetal bovine serum (Gibco™ 26400044) at 37 °C for 12 h under 5% CO<sub>2</sub> atmosphere. Samples had been analyzed spectrophotometrically at excitation and emission wavelengths of 535 nm and 587 nm, respectively. A reference curve has generated using 2-deoxyglucose-6-phosphate without cells. RPMI-1640 supplemented with 10% fetal bovine serum

### **2.4. Lactate Assay**

The detection of the lactate amount produced has been carried out using 25 µL of the collected medium of RPMI 1640 Medium and combined with NADH solution (100 µL, 0.03% of reduced NAD in phosphate buffer) and pyruvate solution (25 µL, 22.7 mM pyruvic acid in phosphate buffer) at RT. The amount of consumed NADH was quantified for each 2 min *via* measuring the absorbance at 340 nm. The mean absorbance was calculated as a percent (%) of the cell-induced via 500 uM NMDA. Each treatment was examined with five repeats and replicates.

### **2.5. ATP Assay**

The estimation of produced cellular ATP has been carried out using a luciferase-based ATP kit

(Abnova™ ATP) to detect the activity of the curcuminoid derivatives in energy depletion in the cancer cells. The principle of the assay depending upon the phosphorylation of glycerol and fluorometric estimation at ( $E_x/E_m = 535/587$  nm). Cells were washed twice with ice-cold PBS followed by 2.5% (w/v) trichloroacetic acid. Then, cells were collected and centrifuged at 9,000 rpm for 5 min at 40 °C, forming supernatant which was diluted and neutralized using tris-acetate buffer (pH 7.7). The ATP content was calculated in the curcuminoid-treated cancer cells in comparison to ones supplemented with a standard ATP inhibitor (oligomycin, 1 μm). Analysis has been carried out using a microplate reader (Multiskan-Thermo Scientific).

## 2.6. Western blot analysis

The current study investigated the expression of proteins in a time-dependent manner after 36 h for (TNF-R1, DR4, DR5, and TRAIL) and 48 h for (Caspase 8, Caspase 3, P53, Bax) after the execution of the treatments with FLLL49-GbA and Ag(I)FLLL49-GbA. Cells were cultured in DMEM medium (Gibco™#31053028) containing the IC<sub>50</sub> concentration values of FLLL49-GbA and Ag(I)FLLL49-GbA in each cell type (MCF-7 and A549). After 24 h incubation, the adherent and floating cells were collected and lysed in RIPA lysis buffer on ice for 30 min. Samples were centrifuged at 12,000 rpm at 4 °C for 10 min. The amount of protein was measured by the BCA protein assay kit (cell signaling technology# 23225). The same amounts of protein were separated using 12.5% SDS polyacrylamide gels and transferred to PVDF membrane (IPVH00010, Merck Millipore). The membrane was blocked with 5% skim milk in PBST (PBS with 0.05% Tween-20) for 30 min at room temperature and then probed with primary antibody dilution overnight at 4 °C. TNF-R1 (D3I7K) (1:1000; Cell Signaling Technology #13377), Anti-DR4 antibody (1:1000, Genetex# GTX66667), anti-DR5 (1:500; MyBioSource# MBS820154), TRAIL Polyclonal antibody (1:500 MyBioSource# MBS852570), Caspases 8 (1:1000; Bioss# bsm-33190M), anti-P53 (1:1000; Diagenode#C15410083), and anti-Bax (1:500; Biorbyt#orb224395). After blotting the PVDF membrane was washed with PBS and covered with the specific secondary antibody for 2 h at room temperature. After three washes, protein bands were captured by a chemiluminescence (ECL) kit (Thermo Scientific (Cat# 31000)). All expressions have been carried out in comparison to β actin expression.

## 2.7. Detection of early and late apoptotic cells

DNA binding dyes Acridine orange (AO) and Ethidium bromide (EtBr), were used for the morphological detection of viable, apoptotic, and necrotic cells. AO is taken up by both non-viable and viable cells that emit green fluorescence when intercalated into DNA. EtBr is taken up only by nonviable cells whereas; it is excluded by viable cells and emits red fluorescence by intercalation into DNA. Cells were seeded on the cover slides inside a six-well plate. Cells were incubated in a CO<sub>2</sub> incubator (5% CO<sub>2</sub>) at 37 °C for 24 h, then treated with IC<sub>50</sub> concentration of each compound and

incubated for 48 h. Cells were washed with cold 1X PBS for three times. Cells were stained with a mixture of AO (100  $\mu\text{g/ml}$ )/ EB (100 $\mu\text{g/ml}$ ) in PBS (1x) with 10% FBS for each well and then incubated for 5 min at RT. The cover slides with cultured stained cells were transferred immediately to new slides and the cells were ready to be visualized by the blue filter of the fluorescence microscope [36,37]. Additionally, the encapsulated Ag(I)FLLL49-GbA complex with CNPs has only been detected for its ability to induce apoptosis.

## 2.8. Anti-inflammatory activity of the novel curcuminoid derivatives

The anti-inflammatory activity of novel compounds was assayed by the method described in the commercial TNF- $\alpha$ , IL-6, and IL1 $\beta$  ELISA kit purchased from Ray Biotech, USA. The expression level was measured by the enzyme-linked immunosorbent assay (ELISA), using their specific pre-coated microplates (12  $\times$  8 microwell strips). Absorbance was measured immediately at 450 nm against blank using an ELISA reader (RayBiotech, Canada). The study of the anti-inflammatory cytokines was carried out in the time interval basis from 3 - 24 h after treatments.

## 2.9. Statistical Analysis

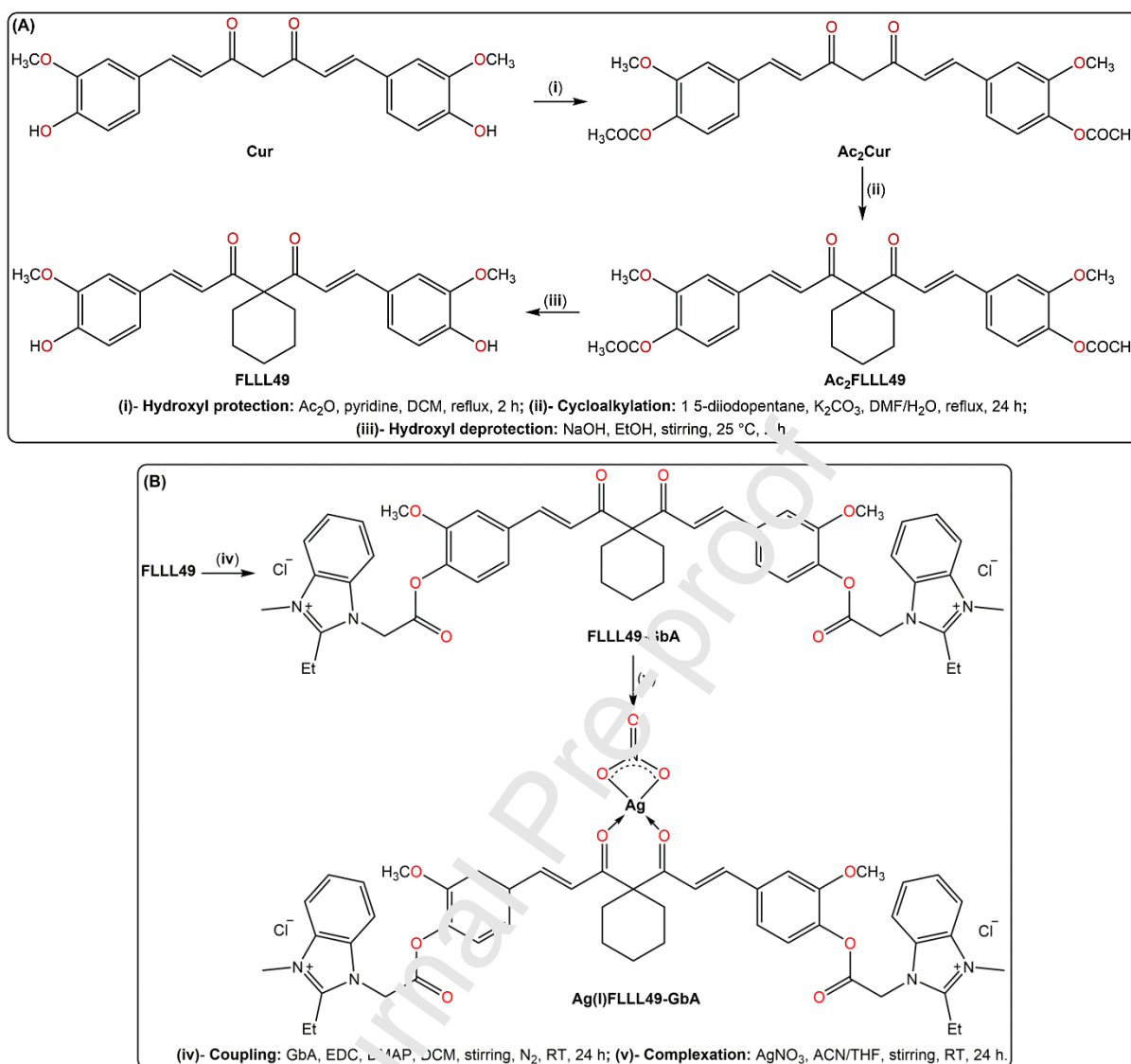
All data between two groups were analyzed using Student's t-test and more than two groups have been conducted using a one-way analysis of variance (ANOVA) followed by Bonferroni tests. Additionally, all data have been expressed as means  $\pm$  standard errors (SEs), and  $P < 0.05$  was considered significant.

## 3. Results and Discussion

### 3.1. Chemistry

The novel conjugate (FLLL49-GbA) and its silver (I) complex (Ag(I) FLLL49-GbA) were synthesized in a three-phases protocol. The first phase involves the preparation of a key starting material, 1,7-Bis(4-hydroxy-3-methoxyphenyl)-4-cyclohexyl-hepta-1,6-dien-3,5-dione (FLLL49), starting from curcumin (Cur) through three consecutive chemical reactions (**Scheme 1A**). Initially, esterification using acetic anhydride was employed to protect the terminal hydroxyl groups of Cur molecule, afterward, cycloalkylation of the methylene group in heptadione fragment by reaction with 1,5-diiodopentane in presence of anhydrous  $\text{K}_2\text{CO}_3$  to produce diacetoxo derivative of FLLL49 ( $\text{Ac}_2\text{FLLL49}$ ), eventually, basic hydrolysis of  $\text{Ac}_2\text{FLLL49}$  to afford free FLLL49. The second phase dedicated to the preparation of 1-(carboxymethyl)-2-ethyl-3-methyl-1H-benzo[d]imidazol-3-ium chloride (Gboxin-analogue, GbA), a key bioactive reagent used for FLLL49 structural refinement. Where 2-Ethylbenzimidazole (EBI) was used as a substrate for the preparation of GbA *via* N-methylation followed by quaternization reactions using methyl iodide and chloroacetic acid, respectively. In the final phase, carboxy terminal of GbA was coupled with the hydroxy terminals of FLLL49 using 1-Ethyl-3-(3'-dimethylaminopropyl) carbodiimide (EDC) and 4-dimethylamino-

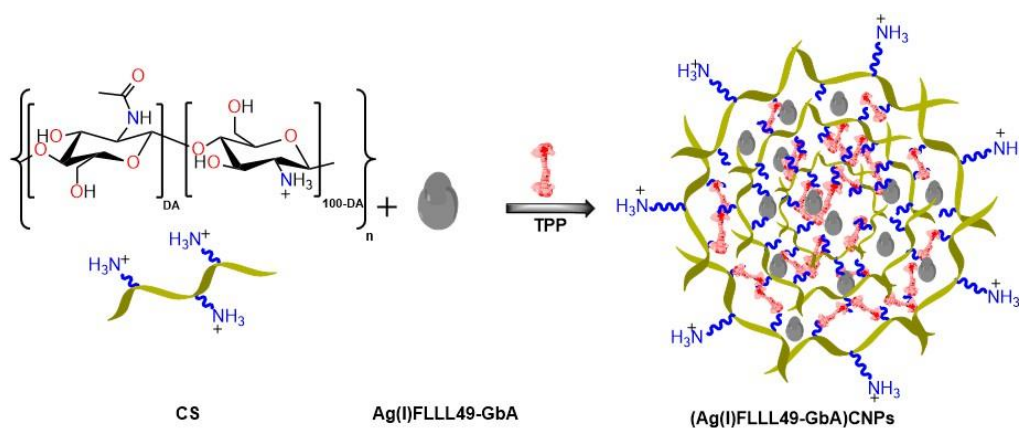
pyridine (DMAP) as a mixed-coupling agent to form FLLL49-GbA conjugate (**Scheme 1B**).



**Scheme 1:** Stepwise protocol for the synthesis of; **(A)** 1,7-Bis(4-hydroxy-3-methoxyphenyl)-4-cyclohexylhepta-1,6-dien-3,5-dione (FLLL49), **(B)** Gboxin analogue (GbA)-based FLLL49 conjugate (FLLL49-GbA) and its silver(I) complex (Ag(I)FLLL49-GbA).

Finally, Ag(I)FLLL49-GbA complex was prepared simply by the reaction of FLLL49-GbA with  $\text{AgNO}_3$  under the ambient conditions. On the other hand, the physical cross-linking protocol was used to convert cationic chitosan (has  $\text{NH}_3^+$  groups that formed in acidic medium) into chitosan nanoparticles (CNPs). In this context, CNPs were prepared by the ionic gelation of cationic chitosan with polyanionic sodium tripolyphosphate (TPP) at room temperature [38]. The ionic gelation occurs through the mutual electrostatic interactions between the cationic and anionic charges of chitosan and TPP, respectively. In our work, we have performed the ionic gelation experiment in the presence of Ag(I)FLLL49-GbA complex which results in the encapsulation of complex by CNPs (see **Scheme 2**). This to take the full therapeutic benefit of the Ag(I)FLLL49-GbA complex and to overcome its side

effects to magnifying its usage pharmacological applications.



**Scheme 2:** One step effective encapsulation of Ag(I)FLLL49-GbA complex with chitosan nanoparticles (CNPs)

## 3.2. Structural characterizations

### 3.2.1. Fourier-transform infrared (FTIR) spectroscopy

The changes in the FTIR spectral features of FLLL49-GbA in comparison to the starting materials (FLLL49 and GbA) (**Fig. 1A**) could provide preliminary spectral evidence for its successful synthesis. To name a few, the coexistence of the common absorption bands characteristic for both FLLL49 (3027  $\text{cm}^{-1}$ , aromatic C-H; 2995 and 2877  $\text{cm}^{-1}$ ,  $\text{CH}_3$  and  $\text{CH}_2$ ; 1674  $\text{cm}^{-1}$ , C=O) and GbA (1580, 1534 and 1386  $\text{cm}^{-1}$ , C=N and C=C groups of benzimidazolium moiety) in the FTIR spectrum of FLLL49-GbA confirms its formation.

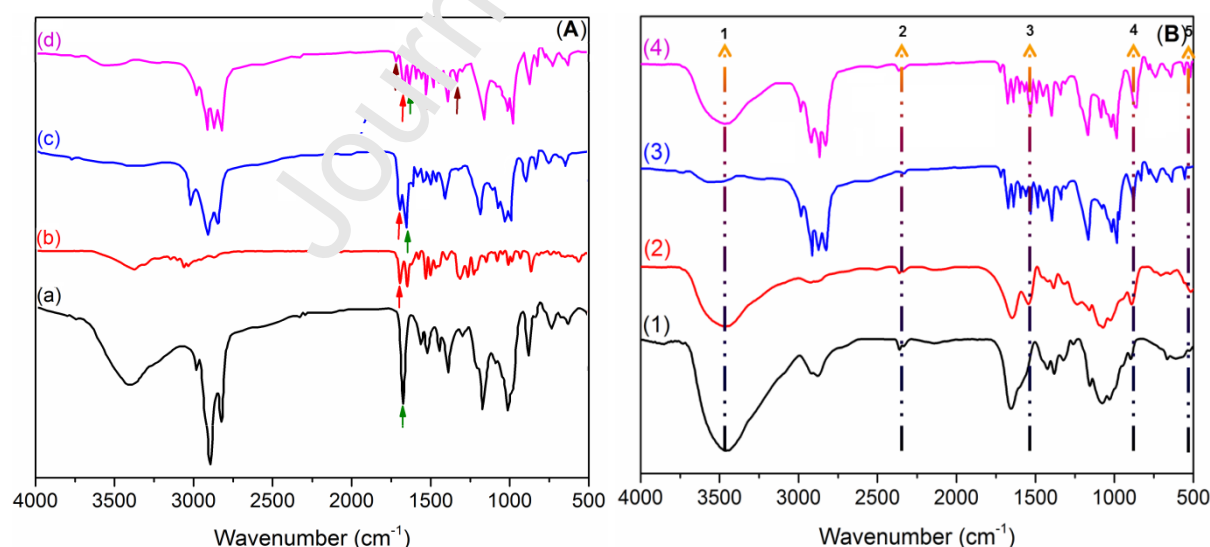


**Fig. 1:** FTIR spectra of (A) key starting materials; (a) 1-(carboxymethyl)-2-ethyl-3-methyl-1H-benzo[d]imidazol-3-ium chloride (Gboxin-analogue, GbA); (b) 1,7-Bis(4-hydroxy-3-methoxyphenyl)-4-cyclohexyl-hepta-1,6-dien-3,5-dione (FLLL49); (c) FLLL49-GbA conjugate; and (d) Ag(I)FLLL49-GbA complex. (B) (1) chitosan (CS); (2) chitosan nanoparticles (CNPs); (3) Ag(I)FLLL49-GbA complex; and (4) encapsulated Ag(I)FLLL49-GbA complex ((Ag(I)FLLL49-GbA)CNPs).

Meanwhile, the disappearance of the broad vibrational band centered at  $\sim 3400\text{ cm}^{-1}$  (attributable to the vibration phenolic and carboxylic OH groups in FLLL49 and GA) along with the emergence of a new stretch at  $1734\text{ cm}^{-1}$  (ascribed to C=O group of ester fragment) prove the coupling of FLLL49 with GA through an ester bond. Importantly, the most significant spectral changes observed in the spectrum Ag(I)FLLL49-GbA as compared to that of parent FLLL49-GbA are; (i) the negative shift of the carbonyl stretch ( $\Delta\nu = -14\text{ cm}^{-1}$ ) coupled with its weakness, attributable to its participation in chelation of Ag(I) ion. (ii) The emergence of a set of new absorption bands at 1767, 1585, 1539, and  $1386\text{ cm}^{-1}$  confirm the involvement of nitrate anion ( $\text{NO}_3^-$ ) in the coordination sphere of Ag(I) ion. Since the frequency gap between the vibration modes  $\nu_4$  ( $1585\text{ cm}^{-1}$ ) and  $\nu_1$  ( $1386\text{ cm}^{-1}$ ) of  $\text{NO}_3^-$  group is  $\sim 200\text{ cm}^{-1}$ , thus,  $\text{NO}_3^-$  is coordinated to Ag(I) ion as a bidentate chelating ligand (**Scheme 1B**) [39].

### 3.2.2. Nuclear magnetic resonance (NMR) spectroscopy

$^1\text{H}$  NMR spectral data GbA, FLLL49, and FLLL49-GbA provide several strong pieces of evidence for the successful coupling between GbA and FLLL49 to form FLLL49-GbA conjugate. To name a few, the emergence of two sets of proton signals distinctive for GbA and FLLL49 in the spectrum of FLLL49-GbA (**Fig. 2**) offers the first evidence; (i) The foremost set was observed at chemical shifts of (ppm) 1.42 (3H), 2.54 (2F), 2.96 (3H), 5.27 (2H), and the range of 7.11-8.51 (2H) attributable to the protons nuclear resonances of ethyl, methyl, methylene, and aromatic fragments of the Gboxin analog (GbA) molecule [53].

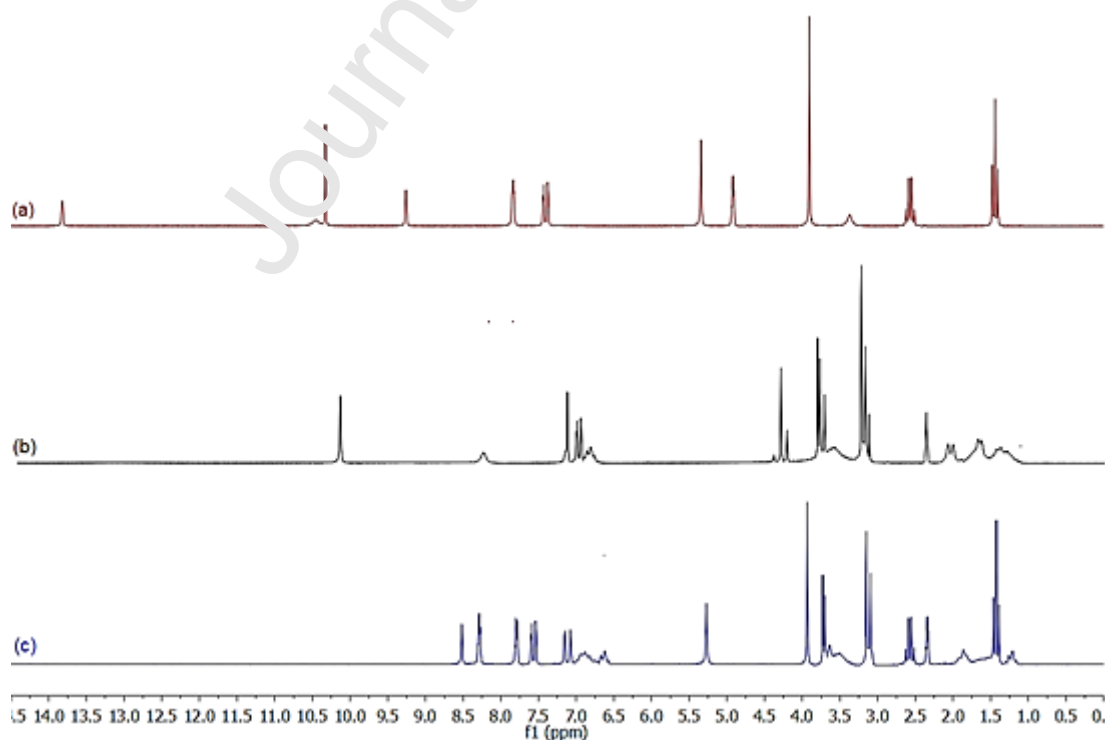


**Fig. 2:**  $^1\text{H}$  NMR spectra of (a) 1-(carboxymethyl)-2-ethyl-3-methyl-1H-benzo[d]imidazol-3-ium chloride

(Gboxin-analogue, GbA); (b) 1,7-Bis(4-hydroxy-3-methoxyphenyl)-4-cyclohexyl-hepta-1,6-dien-3,5-dione (FLLL49); and (c) FLLL49-GbA in  $d_6$ -DMSO.

(ii) The second group of proton signals which are characteristic for FLLL49 molecule was observed at the chemical shift values (ppm): 1.42 – 1.86, 3.74, 6.58-8.52 ppm assignable for the protons nuclear resonances of cyclohexyl, methoxy, olefinic and aromatic fragments of FLLL49. Meanwhile, in comparison to the  $^1\text{H}$  NMR spectra of GbA and FLLL49 (**Fig. 3**), the disappearance of the carboxylic COOH phenolic OH protons in the spectrum of FLLL49-GbA conjugate is indicative of the involvement of these groups in the covalent binding of GbA with FLLL49 through an ester bond.

### 3.2.3. Ultraviolet-Visible (UV-Vis) spectroscopy

The successful formation of Ag(I)FLLL49-GbA along with its stability profile under physiological conditions could be examined based on UV-visible spectroscopy. Where the UV-vis spectrum of FLLL49-GbA ( $10^{-3}$  M) shows two characteristic peaks centered at 262 and 419 nm. On the other hand, four absorption peaks and shoulders were observed in the spectrum of Ag(I)FLLL49-GbA at wavelengths 264, 405, 432, and 457 nm (see **Fig S2, ESI†**). Noteworthy, the higher energy peak distinctive to the  $\pi$ - $\pi^*$  transition for the  $\beta$ - $\alpha$ -carbonyl group of FLLL49-GbA was slightly blue-shifted (419 to 405) as a consequence of its coordination to metal ion [40]. To assess the stability of Ag(I)FLLL49-GbA under physiological parameters, the UV-Vis absorption spectrum of a stocked solution of Ag(I)FLLL49-GbA ( $10^{-5}$  M) in PBS-DMSO buffer (pH = 7.4) was monitored at physiological temperature (37 °C) over a period of 72 h. As shown in **Fig S2**, the storage time has no significant effect on the UV-Vis spectra recorded for the stock solution of Ag(I)FLLL49-GbA with time, supporting the great stability of Ag(I)FLLL49-GbA complex under physiological conditions.

## 3.3. Ag(I)FLLL49-GbA-loaded chitosan nanoparticles

### 3.3.1. Structural and morphological characterization

The FTIR spectra of CS, CNPs, Ag(I)FLLL49-GbA and Ag(I)FLLL49-GbA-loaded chitosan nanoparticles are depicted in **Fig. 1B**. As evident in **Fig. 1B (2)**, three main peaks were observed at 3465, 1646, and 1543  $\text{cm}^{-1}$ , distinctive for CS segment (see **Fig. 1B, (1)**) [41,42], along with notice of new vibration bands 1235 and 1159  $\text{cm}^{-1}$ , characteristic for TPP cross-linker [43]; indicating the successful formation of CNPs. The FTIR spectrum of Ag(I)FLLL49-GbA-loaded chitosan nanoparticles (**Fig. 1B, (4)**) shows the combined absorptions bands of the native Ag(I)FLLL49-GbA complex, chitosan, and TPP cross-linker, however, with some changes in their respective shape, position and intensity due to the physicochemical interactions occurred between these components. To the name few, the characteristic main peaks of the Ag(I)FLLL49-GbA complex 2943, 1734, 1660,

1585, and 1386  $\text{cm}^{-1}$  (**Fig. 1B, (3)**) were observed in the spectrum of its encapsulated form with some distortions, red shifts, and/or decrease in their intensities. Further evidence for the encapsulation of Ag(I)FLLL49-GbA by CNPs is an observation of a new peak around 750  $\text{cm}^{-1}$  in the spectra of encapsulated Ag(I)FLLL49-GbA (**Fig. 1B, (4)**) (characteristic for the out-of-plane bending vibration mode of the imidazolium ring) [44], however, this peak has slightly shifted and decreased in intensity than that in free Ag(I)FLLL49-GbA spectrum (**Fig. 1B, (3)**). Meanwhile, a set of peaks observed at 3461, 1645, 1539, 1234, and 1157  $\text{cm}^{-1}$  (distinctive for CNPs) were also observed in the spectrum of encapsulated Ag(I)FLLL49-GbA with slight alterations in their sites and/or intensities (**Fig. 1B, (2)** and **(4)**). In general, the FTIR results confirm the successful interaction between the Ag(I)FLLL49-GbA and CNPs constituents (CS and TPP) and corroborate the involvement of this silver(I) complex in the nanoparticle formulation.

The surface morphologies of CNPs and Ag(I)FLLL49-GbA-loaded CNPs were investigated based on their respective SEM and TEM images that are given in **Fig. 3 (A-E)**. The SEM image of CS (**Fig. 3A**) revealed a smooth texture with lamellar shape surface. However, the SEM image of CNPs (**Fig. 3B**) shows the spongy nature throughout the surface, providing them accessible cavities available for encapsulation of Ag(I)FLLL49-GbA.

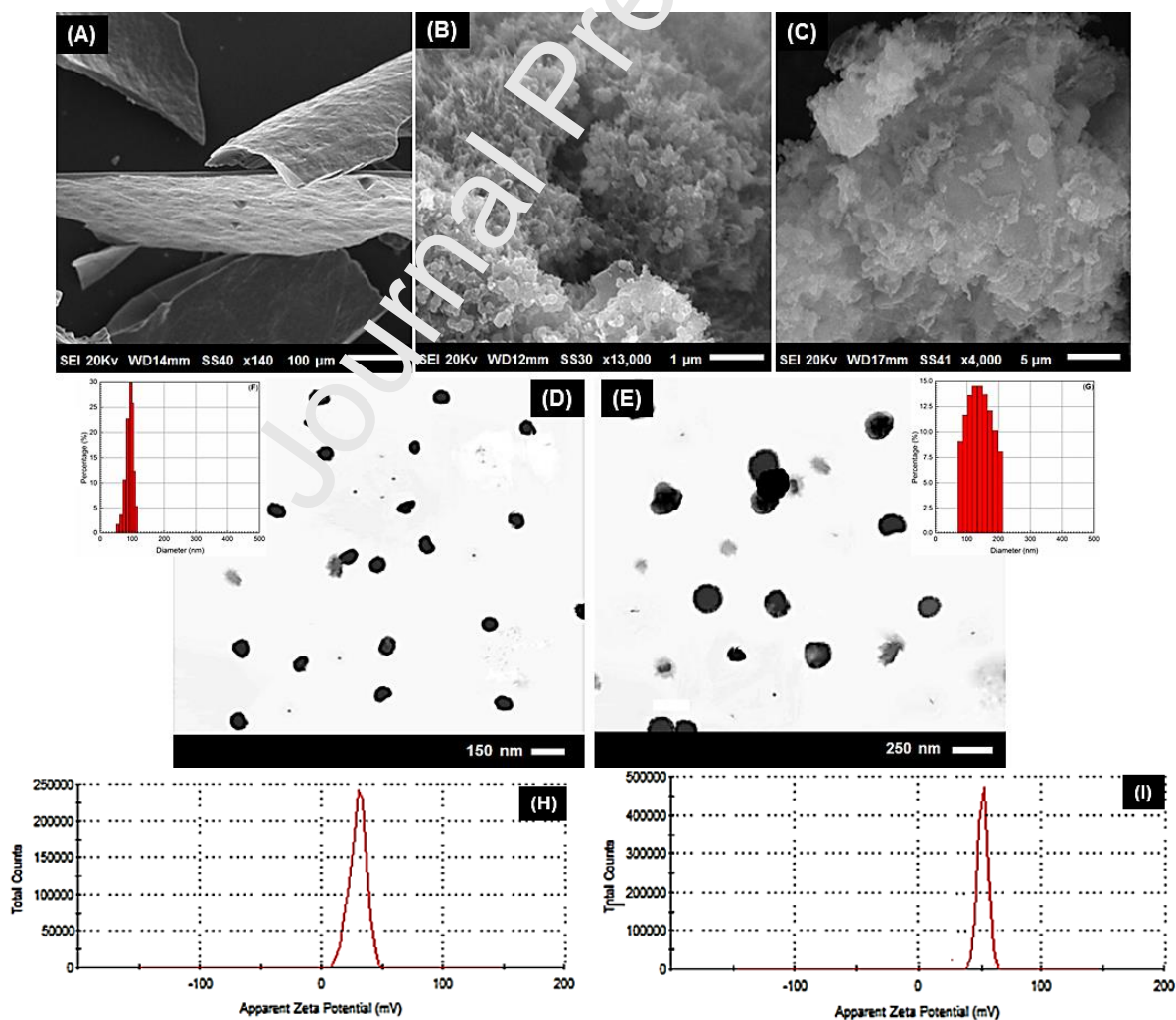


**Fig. 3:** (A-C) Representative SEM images of CS, CNPs, and Ag(I)FLLL49-GbA-loaded CNPs, respectively. (D, E) Representative TEM images of CNPs and (Ag(I)FLLL49-GbA)CNPs; inset graphs (F, G) are DLS-based particle size distribution. (H, I) Zeta potential analysis of CNPs and (Ag(I)FLLL49-GbA)CNPs, respectively.

On the other hand, the SEM micrograph of Ag(I)FLLL49-GbA-loaded CNPs (**Fig. 3C**) displays a fibrous surface with some aggregated structures. Meanwhile, the TEM images (**Fig. 3D, 3E**) showed mono dispersive and homogenous spherical shapes of CNPs and Ag(I)FLLL49-GbA-loaded CNPs, with very few agglomerations in case of (Ag(I)FLLL49-GbA)CNPs. The particle size distributions of native CNPs and Ag(I)FLLL49-GbA-loaded CNPs were determined by dynamic light scattering (DLS) (**Fig. 3F, 3G**; inset graphs in **3D, 3E**, respectively). The DLS results indicated that the diameters of CNPs were in the range of 54.51–112.25 nm with polydispersity indices (PDI) 0.29–0.35, whereas, the diameters Ag(I)FLLL49-GbA-loaded CNPs were ranged from 79.92 nm (PDI 0.32) to 205.63 nm (PDI 0.45). Noteworthy, the low poly-dispersion indices obtained for both nanoparticle formulations are indicative of the narrow size distribution of the nanoparticles in their respective suspension, and consequently formed homogeneous dispersion. This fact could offer plausible explanation for increasing in size, entrapment efficiency, and zeta potential of nanoparticles when they were loaded with Ag(I)FLLL49-GbA as compared to the neat CNPs. The Zeta potentials (ZP) free CNPs and (Ag(I)FLLL49-GbA)CNPs were found to be  $29.8 \pm 0.3$  and  $53.5 \pm 1.2$  mV, respectively (**Fig. 3H, 3I**), which in turns mean that these nanoparticles have enough surface charge to stabilize them against agglomeration. This increasing in zeta potentials of may be attributed to the spreading of cationic imidazolium groups onto the barrier interface of Ag(I)FLLL49-GbA-loaded chitosan nanoparticles [15].

### 3.3.2. Ag(I)FLLL49-GbA loading and encapsulation efficiency

Based on the previous studies related to curcumin-loaded CNPs [29,30], 0.5 mg/mL of Ag(I)FLLL49-GbA was used as an optimum initial concentration to get Ag(I)FLLL49-GbA-loaded CNPs with maximum loading and encapsulation efficiency. The loading and encapsulation efficiency of CNPs for 0.5 mg/mL Ag(I)FLLL49-GbA was found to be 17.9% and 83.5%, respectively. The elevated loading and encapsulation efficacy of CNPs may be due to the spongy nature of their texture which may have helped up-taking a large number of Ag(I)FLLL49-GbA molecules in the nanoparticle core.

### 3.3.3. Ag(I)FLLL49-GbA release kinetics.

The Ag(I)FLLL49-GbA complex-encapsulated CNPs displayed an increased level of complex release from the nanoparticles with time, as the complex was released in the treating medium by 5.8% after 1 h of treatment till reached 45.6% after 24 h of the initial concentration under acidic conditions (ABS, pH 5.3). While under neutral physiological conditions (pH 5), the released concentration was

lowered to start with 2.9% after 1 h till 18.5% after 24 h as shown in **Fig. 4**. Therefore, the acidic pH (5.3) is considered an ideal medium for releasing of the curcuminoid complex form is encapsulated Nano-formulation ((Ag(I)FLLL49-GbA)CNPs) with high activity and bioavailability for its activity in defending and curbing the tumor distribution. The present results were consistent with Popat et al. in their effort to enhance the bioavailability of the curcumin derivatives by encapsulation with nanoparticles; that increase their weak water solubility and rapid intestinal metabolism, ameliorated long-term half-life in circulation which may lead to impressive outcomes for overcoming cancer cell [46].

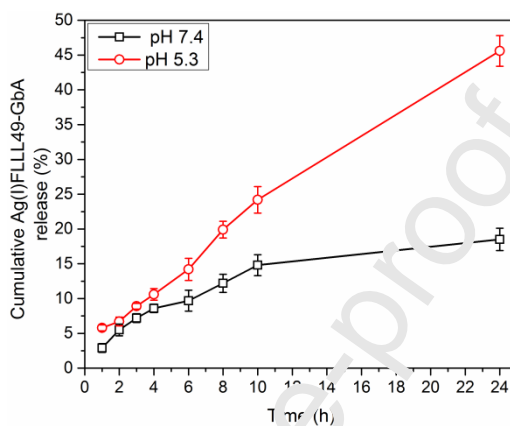


**Fig. 4.** *In vitro* Ag(I)FLLL49-GbA release profiles from CNPs at physiological and acidic conditions (pH 7.4, pH 5.3) at 37 °C. Each point represents the mean  $\pm$  SD ( $p \leq 0.05$ , statistically significant).

Therefore, chitosan nanoparticles were considered as efficient drug delivery carriers for the silver complex owing to their preferable release for this anticancer agent (Ag(I)FLLL49-GbA) in the acidic medium that characteristic for the extracellular environment of cancer cells, thus CNPs increase the specificity and activity of Ag(I) complex for hampering cancer cell spreading [47].

### 3.4. Anticancer study

*In vitro* cytotoxic analysis test of the curcuminoid conjugate (FLLL49-GbA) and its silver(I) complex (Ag(I)FLLL49-GbA) was carried out to detect their safe dose in comparison with a clinical drug (cisplatin (CDDP)), using two human cell lines carcinoma MCF-7 and A549, and normal human cell Hela using a 3-(4,5-dimethylthiazol-2-yl)-2,5-diphenyltetrazolium bromide (MTT) protocol. The cell viability data were graphically represented in **Fig. 5** and the  $IC_{50}$  values of the used compounds were tabulated in **Table 1 (Fig. 5)**. Generally, the parent conjugate presented less cytotoxic action than its Ag(I) complex (Ag(I) FLLL49-GbA) toward all tested cell lines. Just to name a few, FLLL49-GbA and Ag(I)FLLL49-GbA can reduce the viability of MCF-7 cells with a dose-dependent performance (**Fig. 5**) and their respective  $IC_{50}$  values of 164.73 ( $\pm 3.08$ ) and 5.30 ( $\pm 0.21$ )  $\mu\text{g/mL}$ , respectively. therefore, it was obvious to state that the mean activity of Ag(I)FLLL49-GbA against MCF-7 was not only higher than that of FLLL49-GbA with 31-times but also higher than CDDP activity ( $IC_{50} = 10.29 (\pm 0.25) \mu\text{g/mL}$ ) with about 16 times.

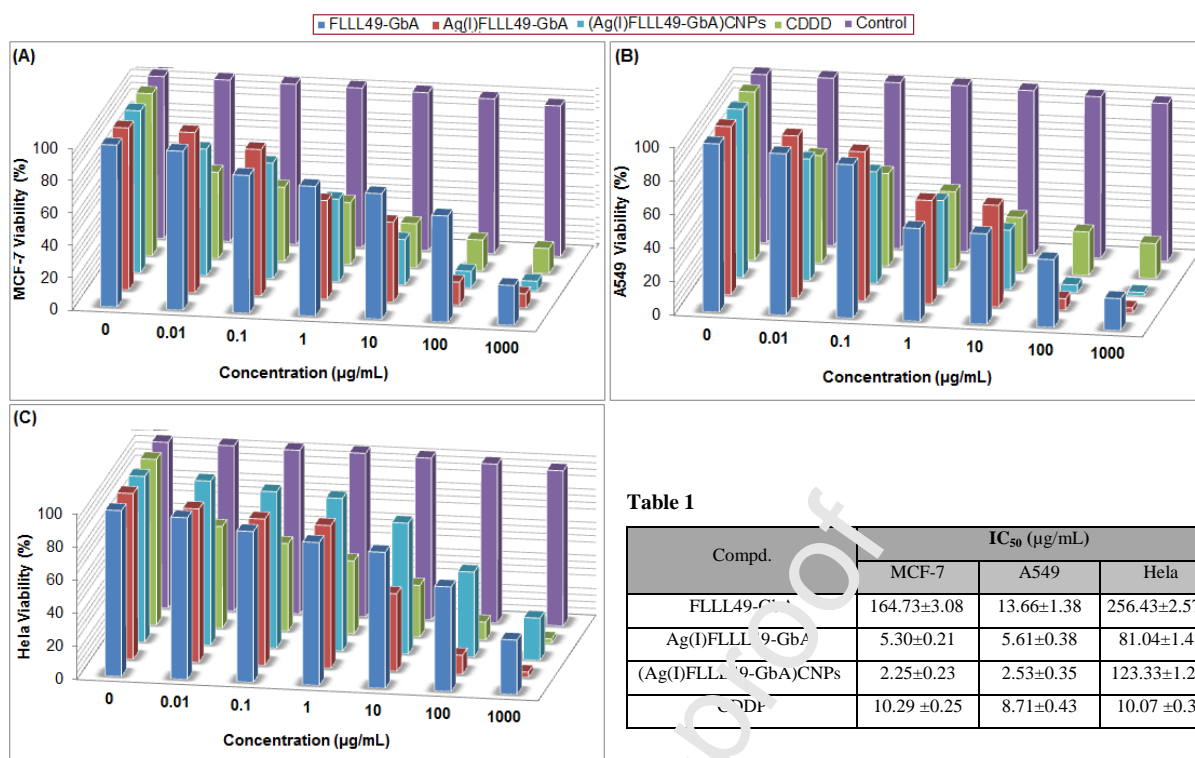


**Fig. 5:** Cell viability of (A) MCF-7; (B) A549; (C) HeLa after 24 h of incubation in presence serial concentrations of FLLL49-GbA, Ag(I)FLLL49-GbA, (Ag(I)FLLL49-GbA)CNP, and cisplatin (CDDP). **Table 1:** IC<sub>50</sub> values (µg/mL) of the tested curcuminoid derivatives in comparison to a clinical drug (CDDP).

To validate the cytotoxicity of the Ag(I)FLLL49-GbA complex-loaded chitosan nanoparticles toward tested cell lines (MCF-7, A549, and HeLa), *in vitro* MTT assay against these cells was conducted. Interestingly, as revealed from the cell viability counts (**Fig. 5**), the cytotoxicity of encapsulated Ag(I) complex was a 1.5-fold increased toward the cancerous cell lines (MCF-7 and A549), contrary, the cytotoxic effect of Nano-formulation has 2-fold diminished against normal cells (HeLa) in comparison to the un-encapsulated complex ( $p \leq 0.05$ ). For instance, at the end of 24 h of treating with 10 mg/mL of free/ encapsulated complex; the still survival MCF-7 and A549 cells were around 49%/ 27% (lower 1.8-time in case Nano-formulation) and 60%/ 35% (lower 1.7-time in case Nano-formulation), respectively. In contrast, the HeLa cells have increased from 46% to 79% after remediation with the free and encapsulated complex, respectively. Thus, the cytotoxicity of Ag(I)FLLL49-GbA complex was significantly increased toward cancer cells (MCF-7 and A549), while, it has reduced toward normal cells (HeLa) when loaded on chitosan Nano-vehicles. This increase in cytotoxicity of the encapsulated Ag(I) complex by CNPs could be ascribed to the enrichment in the internalization of complex-loaded CNPs by an endocytosis mechanism of the Ag(I) complex into the cancerous cells, enhancing its uptake by cancer cells [26]. In addition, chitosan-encapsulated Ag(I)FLLL49-GbA Nano-formulation showed ~2.3-times decrease in IC<sub>50</sub> values as

compared to free Ag(I)FLLL49-GbA after 24 h incubation (**Table 1**).

Although the exact mechanism for the promoted anti-proliferative activity of Ag(I) complexes in comparison to the parent ligands are not well established, it has been proposed that the coordinated silver(I) ion can exert its cytotoxic effect through two possible different mechanisms. The first mechanism involves the binding of Ag (I) ion to thiol groups of proteins and interaction with DNA, inducing apoptosis [48,49]. Additionally, it can interfere with mitochondrial function in cancer cells through interaction of Ag(I) complex with mitochondria and thus stimulating the mitochondrial apoptotic pathway [49]. Furthermore, the greater lipophilicity of Ag(I) complex (Clog P = -0.41) as compared to the parent curcuminoid analog (Clog P = -2.33) increase the extent of binding to the extracellular proteins of cancer cells and enhance its reaction kinetics inside them.<sup>50</sup> Noticeably that the anti-proliferation activity of Ag(I)FLLL49-GbA against MCF-7 cells ( $IC_{50} = 5.30 \pm 0.21 \mu\text{g/mL}$ ) is comparable to that toward A549 cell lines ( $IC_{50} = 5.61 \pm 0.38 \mu\text{g/mL}$ ), however, it is ~2 and ~1.5 times higher than the activity of CDDP toward MCF-7 ( $IC_{50} = 10.2 \pm 0.25 \mu\text{g/mL}$ ) and A549 ( $IC_{50} = 8.71 \pm 0.43 \mu\text{g/mL}$ ), respectively. On the other hand, CDDP is more cytotoxic for normal Hela cell lines ( $IC_{50} = 10.07 \pm 0.36 \mu\text{g/mL}$ ) than Ag(I)FLLL49-GbA ( $IC_{50} = 81.04 \pm 1.48 \mu\text{g/mL}$ ). Therefore, the new chemotherapeutic candidate (Ag(I)FLLL49-GbA) is more effective than the clinical drug (CDDP) in triggering caspases apoptosis in breast and lung cancer cells to prevent their proliferation without health risks.

### 3.5. Performance of new curcuminoid derivatives as apoptosis triggering agents

AO/EtBr staining produced four types of cells that revealed the activity of the conjugate and the complex in inducing apoptosis. As, the normal green nucleus represented the living cells, bright green nucleus with fragmented chromatin represented the cell that are in early apoptotic, orange-stained nuclei with chromatin condensation or fragmentation demonstrated the cells in late apoptotic and necrotic cells were uniformly orange-stained cell nuclei (see **Fig. 6**). On one hand, FLLL49-GbA strongly induced an early apoptotic programmed cell death in A549, MCF7, and HeLa cells with preferable activity toward MCF-7, more than Ag(I)FLLL49-GbA complex, as revealed from high population of the bright green nucleus. On the other hand, Ag(I)FLLL49-GbA is more effective in inducing the late apoptotic pathway with an activity sequence against A549 > HeLa > MCF-7 cells. Additionally, necrotic cells appeared only in the case of treating MCF-7 cells with Ag(I)FLLL49-GbA complex. Moreover, the encapsulated Ag(I)FLLL49-GbA complex with chitosan nanoparticles has induced late apoptotic activity with more effective action than other compounds in the three used cell lines with  $P < 0.05$  as shown in **Fig. 6**.

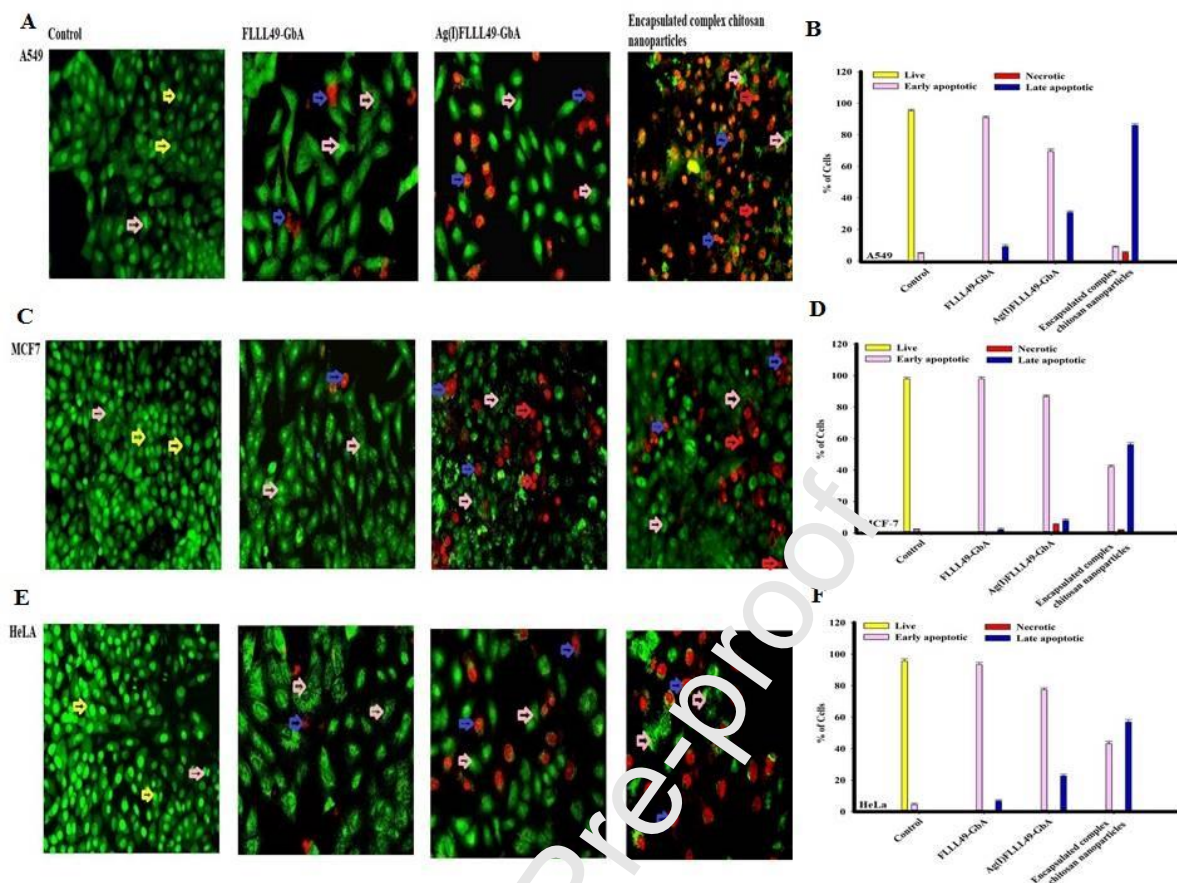


**Fig. 6:** The morphological detection of viable, apoptotic and necrotic cells stained with Acridine orange (AO) and Ethidium bromide (EtBr). A and B) show the effect of FLLL49-GbA, Ag(I)FLLL49-GbA, and encapsulated complex with chitosan nanoparticles on A549 tumor cells and their activity to induce early and late apoptotic cell; C and D) show the effect of FLLL49-GbA, Ag(I)FLLL49-GbA, and encapsulated complex with chitosan nanoparticles on MCF-7 tumour cells and their activity to induce early and late apoptotic cell; E and F) show the effect of FLLL49-GbA, Ag(I)FLLL49-GbA, and an encapsulated complex with chitosan nanoparticles on HeLa cells and their activity to induce early and late apoptotic cell. The presence of late apoptotic cells; nuclei condensation, as demonstrated by acridine orange/Ethidium bromide staining at 200X. Yellow arrows indicate live cell, pink arrows indicate early apoptotic, red arrows indicate necrotic and blue arrows indicate late apoptotic cells.

### 3.6. Inhibitory effects of FLLL49-GbA and Ag(I)FLLL49-GbA on energy indices

The present study attempted to provide a model for controlling the malignancy among cancer cell lines by attacking their proliferation with new curcuminoid derivatives. These compounds have been designed to induce energy depletion in cancer cells that may enhance the constriction for the essential sources of their vitality and proliferation. Therefore, the inhibitory effects of FLLL49-GbA and Ag(I)FLLL49-GbA on energy indices (glucose uptake, lactate production, and intracellular ATP) have been studied. As shown in **Fig. 7A**, the glucose uptakes were significantly decreased in

both cancer cell lines (MCF-7 and A549) after 24 h of treatment with FLLL49-GbA ( $P < 0.05$ ), in comparison to control cells. On the other hand, the Ag(I)FLLL49-GbA complex induced a high significant severe decrease in glucose uptakes with  $P < 0.001$  (for MCF-7 cells) and  $P < 0.01$  (for A549 cells). Moreover, both curcuminoid derivatives have significantly decrease effects on the level of glucose uptake in both cancer cell types than the CDDP treatment ( $P < 0.05$ ) as shown in **Fig. 7A**. Thus, these novel compounds may induce severe blockage for the glucose transporters that responsible for enhancing the uptake of the glucose molecules. The obtained results have supported the suggestion of Cho et al. who suggested that the up-regulation of glucose transporters (GLUT) would contribute to increased glucose uptake that was considered one of the most prominent characters of serous ovarian carcinoma [51].

Additionally, as lactate is considered one of the most important requirements of cellular energy production for all living organisms and act as a functional initiator for protein, lipids, and nucleic acid that enhances the cellular biosynthesis with ATP generation. The present study discussed the role of the treatments of the novel synthesized curcuminoid derivatives on the produced lactate level that is can be used as another source of the energy required for the proliferation of cancer cells. Additionally, lactate rates of the tumor were associated with the increased metastasis and recurrence of the tumor with poor outcome and stimulation of the inflammatory mediators and angiogenesis [52]. The activity of FLLL49-GbA and Ag(I)FLLL49-GbA showed a significant decrease in lactate production in both remediated cancer cells as compared to control cells with  $p < 0.01$  and  $P < 0.001$ , respectively as shown in **Fig 7B**. Moreover, their activity in inhibition lactate production was higher than the cisplatin ( $P < 0.05$ ). Interestingly, these results were considered as supportive with previous research documented by Elshaarawy et al.<sup>53</sup> who revealed that the activity of Pd(II) complex of Gboxin analog-chitoooligosaccharides conjugate (Pd(II)COS@GbA) had an effective role in the depletion of energy production through its activity in the disruption of the ATPase expression.

Prominently, Ag(I)FLLL49-GbA has promising effects in inducing glucose uptake reduction (49% and 80% reduction among MCF-7 and A549 cell lines, respectively) and decreasing lactate production, an essential glycolysis product, (decrease by 61% and 56% for MCF-7 and A549, respectively).

Noteworthy, the positively-charged ends of new curcuminoid derivatives could act as active sites to specifically bind and block the negatively-charged lactate anions which highly secreted across the plasma membrane of proliferated cancer cells as a result of increased glycolysis process [54]. So, the positive charge can offer the specificity and sensitivity of these compounds toward the cancer cells more than normal cells.

As the main aim of this study was to explore novel anticancer candidates able to induce malfunction of energy supply sources of the cancerous cell, that help them to sustain their proliferation and disrupt the inflammatory system.. So, the capacity of the new curcuminoid derivatives to inhibit energy production expressed as intracellular ATP was assessed in comparison

with a standard ATP-production inhibitor (oligomycin, 1 $\mu$ m). On one hand, as shown in **Fig. 7C**, oligomycin, and cisplatin treatment have inhibited the intracellular ATP production with a significant level of  $P < 0.01$  and  $P < 0.05$ , respectively.. On the other side, FLLL49-GbA and Ag(I)FLLL49-GbA showed a significant decrease in the produced ATP with  $P < 0.01$  and  $P < 0.001$ , respectively to both cancer cell lines (MCF-7 and A549). Additionally, it was obvious that the novel compounds have an effective role in the deprivation of the possible sources of energy production and decreased level of ATP which was correlated with the decreased glucose uptake and lactate production by the cancer cell. Furthermore, the present study revealed that the novel curcuminoid derivatives enhanced the inhibition of the energy sources through glycolysis that may trigger the eradication of tumor cell proliferation. Additionally, the novel synthesized compounds triggered the apoptotic actions in the form of early, late apoptosis, and necrosis in both cell types as shown in **Fig. 6**.

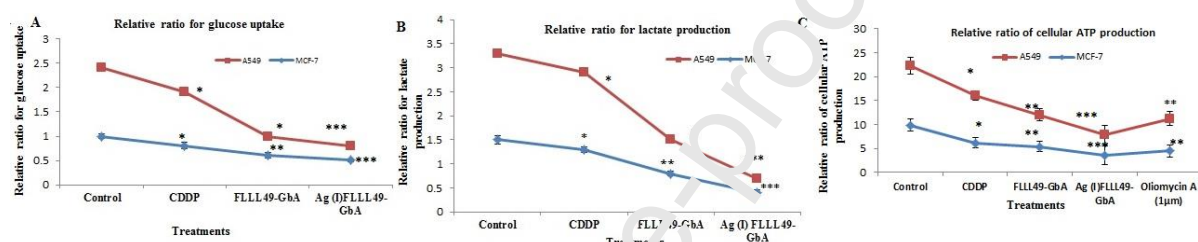


**Fig.7:** The role of novel synthesized FLLL49-GbA and Ag(I)FLLL49-GbA and cisplatin (CDDP) on the level of glucose uptake, lactate production, and ATP produced on MCF-7 and A549 tumor cell lines: A) relative ratio of glucose uptake; all cultural media has been supplemented with 11mM glucose B) Relative ratio of lactate production; C) relative ratio of intracellular produced ATP; Error bars represent  $\pm$ S.E., \* $p < 0.05$ , \*\* $p < 0.01$ , Student's  $t$  test. All experiments were repeated at least 5 times.

Therefore, our results were mostly agreed with Shiratori et al., Eguchi et al., and Nicotera et al. who reported that cell death induction is associated with changes in mitochondrial produced ATP levels [55,56,57], and this incidence can occur in various ways based on the ATP level decrease in the cell that has been shown in several cell types to trigger apoptosis [53,58].

### 3.7. The anti-inflammatory activity of FLLL49-GbA and Ag(I)FLLL49-GbA.

For more profound details of the mechanistic role of the novel synthesized compounds in the treatment of the cancer cell and metastasis; the present study showed that the enhancement of the anti-inflammatory activities was important for controlling the cancer cell proliferation to fence the body homeostasis. Moreover, the present study proposed that the inflammatory stress in the cancer cells and the role of the treatment in the down-regulation of the inflammatory mediators were in time-dependent action. Also, the release of various pro-inflammatory, oncogenic mediators like IL-1 $\beta$ , interleukin-6, and tumor necrosis factor- $\alpha$  (TNF- $\alpha$ ) facilitate the elucidation of the tumor microenvironment. Firstly, Ag(I)FLLL49-GbA complex showed a highly significant effect on the

produced pro-inflammatory cytokines and oncogenic mediators such as TNF- $\alpha$ , IL1 $\beta$ , and IL6 as illustrated in **Fig. 8**. It was revealed that A549 cells are more sensitive than MCF-7 cells; Ag(1) complex have induced significant decrease for TNF- $\alpha$  in comparison to untreated cells and cisplatin treatment for both cell lines (MCF-7 and A549) after the 3rd hour of the treatments with  $P < 0.01$  to  $P < 0.001$ , respectively, as shown in **Fig 8A**.

Secondly, interleukin-6 (IL-6) is considered as one of the most pro-inflammatory cytokines characterizing the disturbance of inflammation in cancerous cells and playing a central role in the expansion and differentiation of the tumor. The treatment with both new compounds for MCF-7 and A549 cancer cells has a significant putative inhibitory effect on the pro-inflammatory factor IL-6 with  $P < 0.001$  6 h post-treatment (**Fig 8b**) in comparison to cisplatin that induced down-regulation for the IL6 with  $P < 0.05$  for MCF-7 from the 3<sup>rd</sup> hour to 24 h; and  $P < 0.01$  for the 6<sup>th</sup> hour of treatment that increased their down-regulation activity by the 24<sup>th</sup> hour for A549 cell lines. Thirdly, **Fig. 8C** revealed that cisplatin did not effect on the IL1 $\beta$  expression level after 3 h of treatment for MCF-7 and 6 h for A549 cell lines.

Moreover, on one side it was obvious that the treatment with both compounds showed a high inhibitory effect for IL1 $\beta$  expression from the 12<sup>th</sup> hour of treatment with  $P < 0.001$  for both MCF-7 and A549 cell lines. Nevertheless, FLLL49-GbA induced down-regulation of the expression after 12<sup>th</sup> hour with a value of  $P < 0.01$  and  $P < 0.001$  for MCF-7 and A549 cell lines, respectively, while Ag(I) induced reduction effect by  $P < 0.001$  for both carcinoma cell lines. Additionally, the overlapping effect was obvious between the treatment with cisplatin and FLLL49-GbA with  $P < 0.01$  for A549 cell lines from the 3<sup>rd</sup> hour till the 24<sup>th</sup> hour (**Fig 8C**).

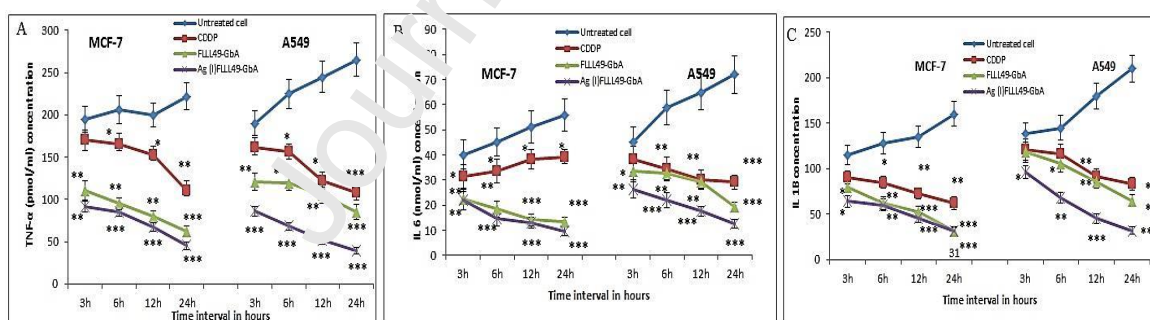


**Fig. 8:** The quantitative anti-inflammatory activity of FLLL49-GbA and Ag(I)FLLL49-GbA and reference drug cisplatin by ELISA on both tumour cell types MCF-7 and A549. **A)** Demonstrate the effect on TNF  $\alpha$  expression; **B)** IL6 expression; **C)** IL1 $\beta$  expression. Error bars represent  $\pm$ S.E., \* $p < 0.05$ , \*\* $p < 0.01$ , Student's  $t$  test. All experiments were repeated at least 5 times.

### 3.8. Putative role of FLLL49-GbA and Ag(I)FLLL49-GbA on activation of death receptors

Caspase activation introduces a dynamic proteolysis cascade in which upstream caspases are exclusively cleaving peptide caspases, which have been progressively further used to facilitate cell

destruction through substrates cleavage [59,60]. Concerning the importance of apoptosis mechanisms in cancer cells, particular attention was paid to the rate of death receptors expression 36 h post-treatment for both cancer cells with the novel synthesized compounds. As death receptors and their ligands are considered important mediators for inducing apoptosis and regulation of tumor proliferation that can be a pivotal therapeutic target for tumor therapy.

Interestingly, in the first 36 h of treatment, the Ag(I) complex has significantly down-regulated the TNF-R1 expression of MCF-7 cells ( $P < 0.01$ ), more than the action of both the parent ligand (FLLL49-GbA) and cisplatin CDDP ( $P < 0.05$ ). Additionally, the activity of the novel curcuminoid derivatives showed significant up-regulation for the TNF-R1 receptor among A549 cell lines. This may reflect the high activity of Ag (I) complex on the breakage of the death domain-containing receptors that allowing the protein-protein interaction leading to inhibiting the TNF- $\alpha$  signaling cascade and its anti-inflammatory action [61]. Therefore, the TNF- $\alpha$  / TNF-R1 interaction has shown close relation to caspases cascade pathways and apoptosis through their antagonistic effects that inhibit or trigger the signaling cascade of the inflammation among cancer cell lines [61].

Additionally, DR4 and DR5 have been significantly up-regulated after 36 h of MCF-7 cell lines treatment. The treatment with FLLL49-GbA conjugate induced significant up-regulation for DR4 and DR5 with a value of  $P < 0.01$  and  $P < 0.05$ , respectively; more than the effect of treatment of Ag(1)FLLL49-GbA complex; while the Ag(I) complex has significant increase for TNF-R1 and TRAIL expressions; both treatments were more effective than the cisplatin treatment (**Fig. 9A,B**). Through reporting its capacity in cancer cell death induction, TRAIL (TNF-related Apoptosis-Inducing Ligand) has developed a growing interest in oncology and tumorigenesis. Mérimo et al. proposed that TRAIL and TRAIL derivatives were already have been considered as molecules with substantial anti-tumor action leading to cell death in diverse cancer cells without *in vivo* massive consequence *in vivo* [62]. So, our results concerning TRAIL expression was valuable for the treatment with the synthesized compounds, as Ag(1) complex induced highly significant expression level than the ligand and cisplatin with significant value of  $P < 0.01$  for MCF-7 cells and  $P < 0.001$  for A549 cells as shown in **Fig 9B,C**. Additionally, the Ag(1) complex showed effective up-regulation for the death receptors and TRAIL proteins in A549 cell lines more than that in MCF-7 as follows  $P < 0.01$ ,  $P < 0.01$ ,  $P < 0.001$  for Dr4, DR5, TRAIL, respectively **Fig. 9B,C**. DI Paolo et al. showed that up-regulating TRAIL expression can be used as a factor for tumor regression among cyclophosphamide treated mice [63], and additionally, Quast et al. reported the necessary role of TRAIL expression in triggering the apoptotic mechanisms dependently on Bax protein expression [64].

### **3.9. The potential activity of FLLL49-GbA and Ag(I)FLLL49-GbA on activation of the tumor suppressor proteins P53 and Bax**

Moreover, through the obtained results that reflect the significant impact of the new curcuminoid

derivatives on the tested cancerous cells; so, it was worth studying the effects of these compounds on caspases activation mechanisms and apoptotic proteins, which are considered as the most important mechanisms that explain the role of safe chemotherapy. So, the caspases group (8 and 3) and the apoptotic markers (P53 and Bax) have been estimated 48 h post-treatment with FLLL49-GbA and Ag (1) FLLL49-GbA to study the final effect of these compounds in triggering the apoptosis and inhibition of cell proliferation. The slightly weak expression of caspase 8 proteins in the untreated control cells of MCF-7 and A549 was parallel with the expression of caspases 3, P53, and Bax.

Besides, the Ag(I)FLLL49-GbA induced highly significant up-regulation for caspase 3, tumor suppressor proteins P53, and Bax with a value of  $P < 0.001$  within the 48 h post-treatment of cancer cell lines (MCF-7 (**Fig. 9A,B**) and A549 (**Fig. 9A,C**) in comparison to control untreated cells as shown in **Fig. 9A**. Additionally, caspases activation for apoptosis has been reported with various triggering structural cascade in form of effector caspases that applied in form of caspases 8 that enhance the extrinsic apoptotic [65,66] and caspases 9 to promote intrinsic apoptotic pathways [67]. Besides, McComb et al. reported that the caspases 3 and 7 revealed an important role with complete expression integrity for stimulation of the internal and external apoptosis pathways [68]. The down-regulation has contributed to the decreasing level of the expressional pathway of both caspases 8 and 9 that appeared to be coincident with delayed cytochrome c secretion that may affect the apoptosis feedback action.

The present study revealed that Bax protein and P53 were highly decreased in their expression in both types of carcinoma cells. On the contrary, Perego et al. have shown that cisplatin-induced reduction in Bax protein expression that was closely linked to drug resistance in ovarian carcinoma cells treatment [69]. So, our results revealed valuable results for the treatment of both cancer cell types and avoiding the problem of the drug resistance that always appears among cisplatin-treated carcinoma. Besides that, the above synthesized compounds were associated with the apoptotic Bax protein expression up-regulation [70,71].

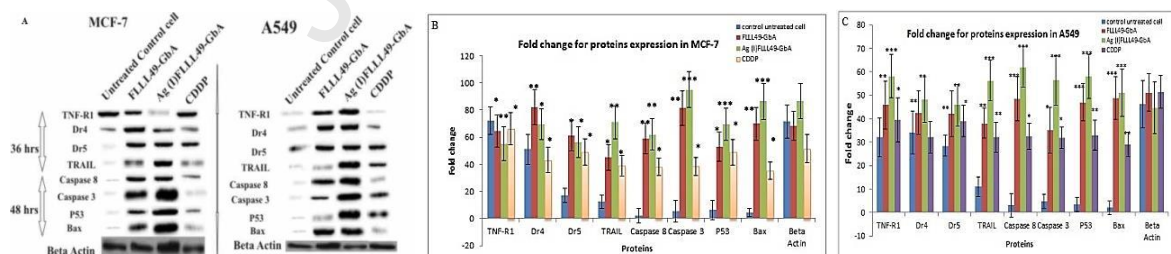


**Fig. 9:** Western blot analysis in MCF-7 and A549 treated with FLLL49-GbA and Ag (I) FLLL49-GbA and reference drug cisplatin after 36hrs and 48hrs of treatments. A) The expression state of TNF-R1, DR4, DR4, TRAIL, Caspases 8 and 9, P53, Bax; B) MCF-7, C) A549, the densitometric analysis of western blotting. Error bars represent  $\pm$ S.E.,  $*p < 0.05$ ,  $**p < 0.01$ , Student's *t* test. All experiments were repeated at least 5 times.

So, activators of Bax expression can, therefore, be used as substitution drugs that improve their expression as a support therapy to facilitate the pro-apoptotic pattern with the order to manage the drug resistance and to increase apoptotic stimuli with tumor reduction [72,73]. Furthermore, an important implication of these findings is that the novel synthesized curcuminoid conjugate and its complex had modified the natural defect of the curcumin treatment through up-regulation of their bioavailability and defending their low aqueous solubility [74]. So, curcumin analogs are considered as a good approach towards boosting curcumin 's bioavailability, several studies have concentrated on developing novel supply systems for the improvement of curcumin pharmacokinetics through encapsulated proteins that had promising anticancer efficiency in MCF-7 cell and high bioavailability in rats [75].

So, the present study tried to improve the applied therapeutic regimes of curcumin applications by increasing their rate of bioavailability and action that can be used as a novel anti-tumor drug that is still under investigation without drug resistance and delude the pleiotropic dysfunction signaling of apoptosis.

So, the novel synthesized curcuminoid conjugate and its Ag(I) complex represented promising candidates to be used alone or in combination together with other therapies as an effective anti-cancer medication. It impacts negatively on numerous signaling pathways and molecular targets that result in the inhibition of cancer growth and proliferation.

## Conclusion

The findings of our research are quite convincing, and thus the following conclusions can be drawn; 1) the activity of curcumin macromolecule with Gboxin and its complex with Ag (I) have the ability to control breast and lung cancer cell depending upon their action on the depletion of the intracellular ATP altogether with the glucose and lactate production. 2) Both derivatives have the ability to direct cancer cell to apoptotic pathway through time-dependent behavior by inhibition of the inflammatory cytokines and up-regulation of the death receptors within 36 hours of treatments and apoptotic caspases such as caspases 3 and caspases 8 with 48 hours of treatment. 3) Additionally, the findings are quite convincing through the ability of the novel synthesized compounds to induce cancer cell apoptosis and cell death through P53 and Bax expression up-regulation. 4) Finally, the study offered a new method to overcome the problems of the natural curcumin characters such as bioavailability and solubility to ameliorate their activity in defending cancer cell proliferation. Moreover, application of encapsulated Ag(I) complex with chitosan nanoparticles (CNPs) significantly triggered apoptosis for cancer cells with low cytotoxicity for HeLa normal cells with released rate at PH medium of 5.3 more than 7.4 with beneficial cancer-targeted drug delivery and hampering cancer cell spreading. Based on the promising findings presented in this research, it was valuable to clear out that the curcumin Ag (I) complex has a potential action activity more than the curcumin conjugate and may provide new perspectives for the development of novel chemotherapies

with less drug resistance for adjunctive treatments of breast and lung cancer cells.

#### **Appendix A. Supplementary data**

Supplementary data (experimental and spectral data) associated with this article will be found, in the online version, at doi:

#### **Compliance with ethical standards**

**Conflict of interest** all authors contributed equally to the production of the manuscript and show no conflict of interest.

**Funding** The authors extend their appreciation to the Dean of Scientific Research at King Khaled University for supporting this work through general research project fund under grant number (**G. R. P / 124 / 41**).

**Ethical approval** this article does not contain any studies with human participants or animals performed by any of the authors.

#### **References**

**Author statement**

**Serag Eldin I. Elbehairi;** Conceptualization, Methodology, Software, Data curation, Validation, Visualization, Writing - Original Draft.

**Lamia A. Ismail;** Conceptualization, Methodology, Software, Data curation, Validation, Visualization, Writing - Original Draft.

**Mohammad Y. Alfaif;** Conceptualization, Software, Data curation, Validation, Visualization, Writing - Original Draft.

**Reda F. M. Elshaarawy;** Conceptualization, Methodology, Software, Data curation, Validation, Visualization, Writing - Original Draft, Writing - Review & Editing

**Hani S. Hafez;** Conceptualization, Methodology, Software, Data curation, Validation, Visualization, Writing - Original Draft, Writing - Review & Editing

- 
- [1] V. Gogvadze, S. Orrenius, B. Zhivotovsky, Mitochondria in cancer cells: what is so special about them?, *Trends Cell Biol.* 18 (2008) 165-173. <https://doi.org/10.1016/j.tcb.2008.01.006>
- [2] B.B. Aggarwal, A. Kumar, A.C. Bharti, Anticancer potential of curcumin: Preclinical and clinical studies, *Anticancer Res.* 23(1A) (2003) 363–398.
- [3] D.K. Agrawal, P.K. Mishra, Curcumin, and its analogues: potential anticancer agents, *Med. Res. Rev.* 30 (2010) 818–860. <https://doi.org/10.1002/med.20088>
- [4] A. Vyas, P. Dandawate, S. Padhye, A. Ahmad, F. Sarkar, Perspectives on new synthetic curcumin analogs and their potential anticancer properties, *Curr. Pharm. Des.* 19 (2013) 2047–2069. DOI : 10.2174/1381612811319110007
- [5] M.A. Tomeh, R. Hadianamrei, X. Zhang, A review of curcumin and its derivatives as anticancer agents, *Int. J. Mol. Sci.* 20(5) (2019) 1033. <https://doi.org/10.3390/ijms20051033>
- [6] B. Salehi, Z. Stojanović-Radić, T. Mitejić, M. Sharifi-Rad, N. V. A. Kumar, N. Martins, J. Sharifi-Rad, The therapeutic potential of curcumin: A review of clinical trials, *Eur. J. Med. Chem.* 163 (2019) 527-545. <https://doi.org/10.1016/j.jmech.2018.12.016>
- [7] P. Yoysungnoen, P. Wachwong, C. Changtam, A. Suksamrarn, S. Patumraj, Anti-cancer and anti-angiogenic effects of curcumin and tetrahydrocurcumin on implanted hepatocellular carcinoma in nude mice, *World J. Gastroenterol.* 14 (2008) 2003-2009. doi: 10.3748/wjg.14.2003
- [8] P. Anand, S.G. Thomas, A.B. Kunnumakkara, C. Sundaram, K.B. Harikumar, B. Sung, S.T. Tharakan, K. Misra, I.K. Priyadarsini, K.N. Rajasekharan, B.B. Aggarwal, Biological activities of curcumin and its analogues (Congeners) made by man and Mother Nature, *Biochem. Pharmacol.* 76 (2008) 1590-1611. <https://doi.org/10.1016/j.bcp.2008.08.008>
- [9] L. Lin, S. Deangelis, E. Foust, J. R. Fuchs, C. Li, P.-K. Li, E.B. Schwartz, G.B. Lesinski, D. Benson, J. Lü, D. Hoyt, J. Lin, A novel small molecule inhibits STAT3 phosphorylation and DNA binding activity and exhibits potent growth suppressive activity in human cancer cells, *Mol. Cancer* 9 (2010) 217. <https://doi.org/10.1186/1476-4598-9-217>
- [10] E.B. Schwartz, The synthesis and optimization of bioactive natural products as anticancer and antileishmanial agents. PhD, Graduate Program in Pharmacy, Ohio State University. (2015).

- [11] M.A. Bill, C. Nicholas, T.A. Mace, J.P. Etter, C. Li, E.B. Schwartz, J.R. Fuchs, G.S. Young, L. Lin, J. Lin, L. He, M. Phelps, P. Li, G. B. Lesinski, Structurally modified curcumin analogs inhibit STAT3 phosphorylation and promote apoptosis of human renal cell carcinoma and melanoma cell lines, *PLoS One* 7 (2012) e40724. <https://doi.org/10.1371/journal.pone.0040724>
- [12] R. Buettner, L.B. Mora, R. Jove, *Clin. Activated STAT signaling in human tumors provides novel molecular targets for therapeutic intervention*, *Cancer Res.* 8 (2002) 945-954.
- [13] T. Kusaba, T. Nakayama, K. Yamazumi, Y. Yakata, A. Yoshizaki, T. Nagayasu, I. Sekine, Expression of p-STAT3 in human colorectal adenocarcinoma and adenoma; correlation with clinicopathological factors, *J. Clin. Pathol.* 58 (2005) 833-838. DOI: 10.1136/jcp.2004.023416
- [14] W.C. Li, S.L. Ye, R.X. Sun, Y.K. Liu, Z.Y. Tang, Y. Kim, J.G. Karras, H. Zhang, Inhibition of growth and metastasis of human hepatocellular carcinoma by antisense oligonucleotide targeting signal transducer and activator of transcription 3, *Clin. Cancer Res.* 12 (2006) 7140-7148. DOI: 10.1158/1078-0432.CCR-06-0484
- [15] M. Pröhl, U.S. Schubert, W. Weigand, M. Gottschaldt, Metal complexes of curcumin and curcumin derivatives for molecular imaging and anticancer therapy, *Coord. Chem. Rev.* 307(1) (2016) 32-41. <https://doi.org/10.1016/j.ccr.2015.09.001>
- [16] K. Murugesan, J. Koroth, P.P. Srinivasan, A. Singh, S. Mukundan, S.S. Karki, B. Choudhary, C.M. Gupta, Effects of green synthesized silver nanoparticles (ST06-AgNPs) using curcumin derivative (ST06) on human cervical cancer cells (HeLa) in vitro and EAC tumor-bearing mice models, *Int. J. Nanomed.* 14 (2019) 5257–5270. <https://doi.org/10.2147/IJN.S202404>
- [17] E. Sheikh, M. B. Bhatt, M. Tripathi, Bio-based synthesized and characterized monodispersed Curcuma longa silver nanoparticles induces targeted anticancer activity in breast cancer cells, *Phcog. Mag.* 14 (57) (2018) 340-345. DOI:10.4103/pm.jm\_71\_18
- [18] S. Garg, A. Garg, Encapsulation of curcumin in silver nanoparticle for enhancement of anticancer drug delivery, *Int. J. Pharm. Sci. Res.* 9(3) (2018) 1160-1166. DOI: 10.13040/IJPSR.0975-8232.9(3).1160-66
- [19] X.X. Yang, C.M. Lia, C.Z. Huang, Curcumin modified silver nanoparticles for highly efficient inhibition of respiratory syncytial virus infection, *Nanoscale* 8 (2016) 3040–3048. <https://doi.org/10.1039/C5NR07918G>
- [20] C.-Y. Loo, R. Rohanizadeh, P.M. Young, D. Traini, R. Cavaliere, C.B. Whitchurch, W.-H. Lee, Combination of silver nanoparticles and curcumin nanoparticles for enhanced anti-biofilm activities, *J. Agric. Food Chem.* 64(12) (2016) 2513-2522. <https://doi.org/10.1021/acs.jafc.5b04559>
- [21] K. Varaprasad, Y.M. Mohan, K. Vimala, K.M. Raju, Synthesis and characterization of hydrogel-silver nanoparticle-curcumin composites for wound dressing and antibacterial application, *J. App. Polymer Sci.* 121 (2011) 784–796. <https://doi.org/10.1002/app.33508>
- [22] H. K. Syed, M. A. Iqbal, R. A. Haque, K.-K. Peh, Synthesis, characterization and antibacterial activity of a curcumin–silver(I) complex, *J. Coord. Chem.* 68(6) (2015) 1088-1100. <https://doi.org/10.1080/00958972.2014.1003051>
- [23] C. Lia, J. Wangb, Y. Wangb, H. Gaoc, G. Weid, Y. Huange, H. Yue, Y. Gane, Y. Wangf, L. Meig, H. Chenh, H. Hui, Z. Zhangj, Y. Jink, Recent progress in drug delivery, *Acta Pharma. Sinica B* 9(6) (2019) 1145-1162. <https://doi.org/10.1016/j.apsb.2019.08.003>
- [24] B. Begines, T. Ortiz, M. Pérez-Aranda, G. Martínez, M. Merinero, F. Argüelles-Arias, A. Alcludia,

- Polymeric Nanoparticles for Drug Delivery: Recent developments and future prospects, *Nanomaterials* 10, (2020) 1403. doi:10.3390/nano10071403
- [25] M.A. Mohammed, J.T.M. Syeda, K.M. Wasan, E.K. Wasan, An overview of chitosan Nanoparticles and its application in non-parenteral drug delivery, *Pharmaceutics* 9(4) (2017) 53. doi: 10.3390/pharmaceutics9040053
- [26] R. Viveka, R. Thangama, V. Nipunabua, T. Ponraja, S. Kannan, Oxaliplatin-chitosan nanoparticles induced intrinsic apoptotic signaling pathway: A “smart” drug delivery system to breast cancer cell therapy *Int. J. Biol. Macromol.* 65 (2014) 289–297. <http://dx.doi.org/10.1016/j.ijbiomac.2014.01.05>
- [27] E.A. El-Alfy, M.K. El-Bisi, G.M. Taha, H.M. Ibrahim. Preparation of biocompatible chitosan nanoparticles loaded by tetracycline, gentamycin and ciprofloxacin as novel drug delivery system for improvement the antibacterial properties of cellulose based fabrics, *Int. J. Biol. Macromol.* 161 (2020), in press, <https://doi.org/10.1016/j.ijbiomac.2020.06.118>
- [28] V.I. Mobarakeh, M.H. Modarressi, P. Rahimi, A. Bolhassani, L. Arefian, F. Atyabi, R. Vahabpour, Optimization of chitosan nanoparticles as an anti-HIV siRNA delivery vehicle, *Int. J. Biol. Macromol.* 129 (2019) 305–315. <https://doi.org/10.1016/j.ijbiomac.2019.02.055>
- [29] S.M. Abdel-Hafez, R.M. Hathou, O.A. Sammour, Tracking the transdermal penetration pathways of optimized curcumin-loaded chitosan nanoparticles via confocal laser scanning microscopy, *Int. J. Biol. Macromol.* 108 (2018) 753–764. <https://doi.org/10.1016/j.ijbiomac.2017.10.170>
- [30] N. Alizadeh, S. Malakzadeh, Antioxidant, antibacterial and anti-cancer activities of  $\beta$ - and  $\gamma$ -CDs/ curcumin loaded in chitosan nanoparticles, *Int. J. Biol. Macromol.* 147 (2020) 778–791. <https://doi.org/10.1016/j.ijbiomac.2020.01.206>
- [31] Y. Shi, S.K. Lim, Q. Liang, S.V. Iyer, J. Y. Wang, Z. Wang, X. Xie, D. Sun, Y.-J. Chen, V. Tabar, P. Gutin, N. Williams, J.K. De Brabandere, L.F. Parada, Gboxin is an oxidative phosphorylation inhibitor that targets glioblastoma, *Nature* 567, 7740 (2019) 341–346. <https://doi.org/10.1038/s41586-019-0993-x>
- [32] M.Y. Alfaiji, M.A.-E. Zein, A.A. Snati, M.A. Alshehri, S.E.I. Elbehairi, H.S. Hafez, R.F.M. Elshaarawy, Synthesis, photophysical behavior and biomolecular reactivity of new triphenylphosphonium-based Pd(II)salphens as new anticancer candidates, *J. Photochem. Photobiol. A: Chem.* 385 (2019) 112083. <https://doi.org/10.1016/j.jphotochem.2019.112083>
- [33] M.Y. Alfaiji, S.E.I. Elbehairi, H.S. Hafez, R.F.M. Elshaarawy. Spectroscopic exploration of binding of new imidazolium-based palladium (II) saldach complexes with CT-DNA as anticancer agents against HER2/neu overexpression, *J. Mol. Struct.* 1191 (2019) 118–128. <https://doi.org/10.1016/j.molstruc.2019.04.119>
- [34] R.F.M. Elshaarawy, T.B. Mostafa, A.A. Refaee, E.A. El-Sawi, Ionic Sal-SG Schiff bases as new synergetic chemotherapeutic candidates: synthesis, metalation with Pd (II) and in vitro pharmacological evaluation, *RSC Adv.* 5 (2015) 68260–68269. <https://doi.org/10.1039/C5RA11083A>
- [35] H. Zhang, J. Jung, Y. Zhao, Preparation, characterization and evaluation of antibacterial activity of catechins and catechins–Zn complex loaded-chitosan nanoparticles of different particle sizes, *Carbohydr. Polym.* 137 (2016) 82–91. <http://dx.doi.org/10.1016/j.carbpol.2015.10.036>
- [36] E.-H. Liu, L.-W. Qi, Q. Wu, Y.-B. Peng, P. Li, Anticancer agents derived from natural products, *Mini Rev. Med. Chem.* 9 (2009) 1547–1555. <https://doi.org/10.2174/138955709790361520>

- [37] F. Albright, R.A. Stephenson, N. Agarwal, C.C. Teerlink, W.T. Lowrance, J.M. Farnham, L.A. Albright, Prostate cancer risk prediction based on complete prostate cancer family history, *J. Korean Med. Sci.* 75 (2015) 390–398. <https://doi.org/10.1002/pros.22925>
- [38] W. Fan, W. Yan, Z. Xu, H. Ni, Formation mechanism of monodisperse, low molecular weight chitosan nanoparticles by ionic gelation technique. *Colloids Surf. B.* 90 (2012) 21–27. <https://doi.org/10.1016/j.colsurfb.2011.09.042>
- [39] I. S. Ahuja, S. Tripathi, G. L. Yadava, Synthesis and characterization of silver(I) nitrate complexes with 2-, 3-, and 4- cyano- pyridines and anilines, *Synth. React. Inorg. Met.-Org. Chem.* 20(2) (1990) 189-198. <https://doi.org/10.1080/00945719008048126>
- [40] Y.-M. Song, J.-P. Xu, L. Ding, Q. Hou, J.W. Liu, Z.-L. Zhu, Syntheses, characterization and biological activities of rare earth metal complexes with curcumin and 1,10-phenanthroline-5,6-dione, *J. Inorg. Biochem.* 103 (2009) 396. <https://doi.org/10.1016/j.jinorgbio.2008.12.001>
- [41] R.F.M. Elshaarawy, F.H.A. Mustafa, A. Herbst, A.E.M. Farag, C. Janiak, Surface functionalization of chitosan isolated from shrimp shells, using salicylaldehyde ionic liquids in exploration for novel economic and ecofriendly antibiofoulants, *RSC Adv.*, 6 (2016) 20901–20915.
- [42] R.F.M. Elshaarawy, F.H.A. Mustafa, L. van Geelen, A.E.A. Abou-Talebe, H.R.Z. Tadrose, R. Kalscheuer, C. Janiak, Mining marine shell wastes for polyelectrolyte chitosananti-biofoulants: Fabrication of high-performance economic and ecofriendly anti-biofouling coatings, *Carbohydr. Polym.* 172 (2017) 352–364. DOI: 10.1016/j.carbpol.2017.05.059.
- [43] A.V. Singh, L.K. Nath, Synthesis and evaluation of physicochemical properties of cross-linked sago starch, *Int J Biol Macromol.* 50 (2012) 14–8. <http://doi.org/10.1016/j.ijbiomac.2011.09.003>
- [44] T. Yamada, M. Mizuno, Characteristic spectroscopic features because of cation–anion interactions observed in the 700–950  $\text{cm}^{-1}$  range of infrared spectroscopy for various imidazolium-based ionic liquids, *ACS Omega* 3(7) (2018) 8027–8035. <https://doi.org/10.1021/acsomega.8b00938>
- [45] R. Safdar, A. Omar, A. Annagiri, M. Thanabalan, Synthesis and characterization of imidazolium ILs based chitosan–tripolyphosphate microparticles, *IOP Conf. Ser.: Mater. Sci. Eng.* 458 (2018) 012080.
- [46] A. Papat, S. Karmakar, S. Jambhrunkar, C. Xu, C. Yu, Curcumin-cyclodextrin encapsulated chitosan nanoconjugates with enhanced solubility and cell cytotoxicity, *Colloids Surf. B.* 117 (2014) 520-527. <https://doi.org/10.1016/j.colsurfb.2014.03.005>
- [47] Z.M. Bhujwalla, D. Artetmov, P. Bllestros, S. Cerdan, R.J. Gillies, M. Solaiyappan, Combined vascular and extracellular pH imaging of solid tumors. *NMR Biomed.* 15 (2002) 114–119. <https://doi.org/10.1002/nbm.743>
- [48] J. Roberts, J.M. Pascoe, Cross-linking of complementary strands of DNA in mammalian cells by antitumour platinum compounds, *Nature* 235 (1972) 282–284. <https://doi.org/10.1038/235282a0>
- [49] C.N. Banti, S.K. Hadjikakou, Anti-proliferative and anti-tumor activity of silver(I) compound, *Metallomics.* 5 (2013) 569-596. <https://doi.org/10.1039/C3MT00046J>
- [50] J.J. Liu, P. Galettis, A. Farr, L. Maharaj, H. Samarasinha, A.C. McGechan, B.C. Baguley, R.J. Bowen, S.J. Berners-Price, M.J. McKeage, *In vitro* antitumour and hepatotoxicity profiles of Au(I) and Ag(I) bidentate

- pyridyl phosphine complexes and relationships to cellular uptake, *J. Inorg. Biochem.* 102 (2008) 303–310. <https://doi.org/10.1016/j.jinorgbio.2007.09.003>
- [51] H. Cho, Y.S. Lee, J. Kim, J.Y. Chung, J.H. Kim, Overexpression of glucose transporter-1 (GLUT-1) predicts poor prognosis in epithelial ovarian cancer, *Cancer Investig.* 31 (2013) 607–615. <https://doi.org/10.3109/07357907.2013.849722>
- [52] P. Sonveaux, F. Végran, T. Schroeder, M.C. Wergin, J. Verrax, Z. N. Rabbani, C.J. De Saedeleer, K.M. Kennedy C. Diepart, B.F. Jordan, M.J. Kelley, B. Gallez, M.L. Wahl, O. Feron, M.W. Dewhirst, Targeting lactate-fueled respiration selectively kills hypoxic tumor cells in mice, *J. Clin. Invest.* 118(12) (2008) 3930–3942. <https://doi.org/10.1172/JCI36843>
- [53] S.E.I. Elbehairi, M.Y. Alfaifi, A.A. Shati, M.A. Alshehri, R.F.M. Elshaarawy, H.S. Hafez, Role of Pd (II)@Chitooligosaccharides@Gboxin analog in oxidative phosphorylation inhibition and energy depletion: targeting mitochondrial dynamics, *Chem. Biol. Drug Des.* in press, 2020. <https://doi.org/10.1111/cbdd.13703>
- [54] D.C. Gadsby, Ion Channels versus ion pumps: the principal difference, in principle, *Nat. Rev. Mol. Cell Biol.* 10 (2009) 344–52. <https://doi.org/10.1038/nrm2668>
- [55] R. Shiratori, K. Furuichi, M. Yamaguchi, Glycolytic suppression dramatically changes the intracellular metabolic profile of multiple cancer cell lines in a mitochondrial metabolism-dependent manner, *Sci. Rep.* 9 (2009) 18699. <https://doi.org/10.1038/s41598-019-55225-3>
- [56] Y. Eguchi, S. Shimizu, Y. Tsujimoto, Intracellular ATP levels determine cell death fate by apoptosis or necrosis, *Cancer Res.* 57(10) (1997) 1835–1840.
- [57] P. Nicotera, M. Leist, E. Ferrando-Ma, Intracellular ATP, a switch in the decision between apoptosis and necrosis, *Toxicol. Lett.* 102–103(8) (1998) 129–142. [https://doi.org/10.1016/S0378-4274\(98\)00298-7](https://doi.org/10.1016/S0378-4274(98)00298-7)
- [58] L. Xiaoping, X. Zizheng, C. Tao, S.H. Liang, G. Huiqin, Glucose metabolism on tumor plasticity, diagnosis, and treatment, *Front. Oncol.* 10 (2020) 317. <https://doi.org/10.3389/fonc.2020.00317>
- [59] E.A. Slee, M.T. Harte, R.M. Kluck, B.B. Wolf, C.A. Casiano, D.D. Newmeyer, H.-G. Wang, J.C. Reed, D.W. Nicholson, E.S. Alnemri, D.R. Green, S.J. Martin, Ordering the Cytochrome c-initiated Caspase Cascade: Hierarchical Activation of Caspases-2, -3, -6, -7, -8, and -10 in a Caspase-9-dependent Manner, *J. Cell Biol.* 144 (1999) 281–292. <https://doi.org/10.1083/jcb.144.2.281>
- [60] U. Fischer, R.U. Jänicke, K. Schulze-Osthoff, Many cuts to ruin: A comprehensive update of caspase substrates, *Cell Death Differ.* 10 (2003) 76–100. <https://doi.org/10.1038/sj.cdd.4401160>
- [61] D.L. Faustman, M. Davis, TNF receptor 2 and disease: Autoimmunity and regenerative medicine, *Front. Immunol.* 4 (2013) 478. <https://doi.org/10.3389/fimmu.2013.00478>
- [62] D. Mérino, N. Lalaoui, A. Morizot, E. Solary, O. Mischeau, TRAIL in cancer therapy: present and future challenges, *Expert Opin. Ther. Targets* 11(10) (2007) 1299–1314. <https://doi.org/10.1517/14728222.11.10.1299>
- [63] N.C. Di Paolo, S. Tuve, S. Ni, K.E. Hellström, I. Hellström, A. Lieber, Effect of Adenovirus-mediated heat shock protein expression and oncolysis in combination with low-dose cyclophosphamide treatment on antitumor immune responses, *Cancer Res.* 66(2) (2006) 960–969. DOI: 10.1158/0008-5472.CAN-05-2388
- [64] S.A. Quast, A. Berger, M. Plotz, J. Eberle, Sensitization of melanoma cells for TRAIL-induced apoptosis by activation of mitochondrial pathways via Bax, *Eur. J. Cell Biol.* 93(1–2) (2014) 42–48.

<https://doi.org/10.1016/j.ejcb.2013.11.003>

- [65] T. Eissing, H. Conzelmann, E.D. Gilles, F. Allgöwer, E. Bullinger, P. Scheurich, Bistability analyses of a caspase activation model for receptor-induced apoptosis, *J. Biol. Chem.* 279 (2004) 36892–36897. doi: 10.1074/jbc.M404893200
- [66] K.S. Ferreira, C. Kreutz, S. MacNelly, K. Neubert, A. Haber, M. Bogyo, J. Timmer, C. Borner, Caspase-3 feeds back on caspase-8, Bid and XIAP in type I Fas signaling in primary mouse hepatocytes, *Apoptosis* 17 (2012) 503–515. <https://doi.org/10.1007/s10495-011-0691-0>
- [67] S. McComb, P.K. Chan, A. Guinot, H. Hartmannsdottir, S. Jenni, M.P. Dobay, J.-P. Bourquin, B.C. Bornhauser, Efficient apoptosis requires feedback amplification of upstream apoptotic signals by effector caspase-3 or -7, *Sci. Adv.* 5 (2019) 9433. DOI: 10.1126/sciadv.aau9433
- [68] S.A. Lakhani, A. Masud, K. Kuida, G.A. Porter, C.J. Booth, W.Z. Mehal, I. Inayat, R.A. Flavell, Caspases 3 and 7: key mediators of mitochondrial events of apoptosis, *Science* 311 (2006) 847–851. DOI: 10.1126/science.1115035
- [69] P. Perego, M. Giarola, S.C. Righetti, R. Supino, C. Caserini, D. Zilia, M.A. Pierotti, T. Miyashita, J.C. Reed, F. Zunino, Association between cisplatin resistance and mutation of p53 gene and reduced bax expression in ovarian carcinoma cell systems, *Cancer Res.* 56(3) (1996) 556–562.
- [70] A.M. Verhagen, P.G. Ekert, M. Pakusch, J. Silke, I. Dowd, Connolly, G.E. Reid, R.L. Moritz, R.J. Simpson, D.L. Vaux, Identification of DIABLO, a Mammalian Protein that Promotes Apoptosis by Binding to and Antagonizing IAP Proteins, *Cell* 102 (2000) 33–43. [https://doi.org/10.1016/S0092-8674\(00\)00009-X](https://doi.org/10.1016/S0092-8674(00)00009-X)
- [71] C. Du, M. Fang, Y. Li, L. Li, X. Wang, Smac, a Mitochondrial Protein that Promotes Cytochrome c-Dependent Caspase Activation by Eliminating IAP Inhibition, *Cell* 102 (2000) 33–42. [https://doi.org/10.1016/S0092-8674\(00\)00009-8](https://doi.org/10.1016/S0092-8674(00)00009-8)
- [72] R.C. Bargou, C. Wagener, K. Bornhauser, M.Y. Mapara, P.T. Daniel, W. Arnold, M. Dietel, H. Guski, A. Feller, H.D. Royer, B. Dorkan, Overexpression of the death-promoting gene bax-alpha which is downregulated in breast cancer restores sensitivity to different apoptotic stimuli and reduces tumor growth in SCID mice, *J. Clin. Invest.* 97(11) (1996) 2651-2659. <https://doi.org/10.1172/JCI118715>
- [73] H. Li, H. Zhu, C.-J. Yu, J. Yuan, Cleavage of BID by caspase 8 mediates the mitochondrial damage in the Fas pathway of apoptosis, *Cell* 94 (1998) 491–501. [https://doi.org/10.1016/S0092-8674\(00\)81590-1](https://doi.org/10.1016/S0092-8674(00)81590-1)
- [74] S.R. Kunati, S.M. Yang, B.M. William, Y. Xu, An LC-MS/MS method for simultaneous determination of curcumin, curcumin glucuronide and curcumin sulfate in a phase II clinical trial, *J. Pharm. Biomed. Anal.* 156 (2018) 189–198. <https://doi.org/10.1016/j.jpba.2018.04.034>
- [75] D. Barone, L. Cito, G. Tommonaro, A.A. Abate, D. Penon, R. De Prisco, A. Penon, I.M. Forte, E. Benedetti, A. Cimini, Antitumoral Potential, Antioxidant Activity and Carotenoid Content of Two Southern Italy Tomato Cultivars Extracts: San Marzano and Corbarino, *J. Cell Physiol.* 233 (2018) 1266–1277. <https://doi.org/10.1002/jcp.25995>